The effect of ions on the motion of an oil slug in a charged capillary

Zachary Wilmott, Christopher Breward, Jonathan Chapman

December 2, 2016

1 Introduction

The process of recovering oil from a reservoir traditionally comprises three stages. When first drilling into a reservoir, the high pressure in the rock forces out hydrocarbons in the form of gases and oils; this process is referred to as primary oil recovery. Eventually, the naturally high pressure in the reservoir drops, and water needs to be injected to maintain the rate at which the oil is retrieved. Typically, seawater is used for this secondary waterflood. However, a high percentage of the oil remains undisturbed, and a tertiary waterflood is often performed to remove some of the oil that can't be recovered using seawater alone. Numerous technologies have been developed for this tertiary recovery stage, such as alkaline flooding, polymer flooding, and gas injection. This paper is motivated by one such technology, namely low salinity waterflooding.

In low salinity waterflooding, low salinity water is injected into the reservoir instead of seawater. Provided certain conditions are met, such as polar compounds being present in the oil, clay compounds being present in the reservoir, and divalent ions being present in the formation water [1], a low salinity waterflood results in additional oil being recovered. While the requirements for low salinity oil recovery to be effective are relatively well known, the dominant causal mechanism is not well understood, and a number of potential mechanisms have been proposed in the literature.

For example, Tang and Morrow [22] suggest that the presence of lower salinity water causes the electrical double layer between the clay platelets present in the reservoir to expand and release fines. These fines act as a surfactant, and alter the permeability of the reservoir. McGuire et al. [21] suggest that, due to the increase in pH during a low salinity injection, the interfacial tension is reduced, leading to a wettability alteration. As a secondary effect, they claim that the carboxylic compounds in the oil are desorbed from the clay as a result of the pH increase.

Lager et al. [15] propose an alternative mechanism, known as Multicomponent Ionic Exchange (MIE). In this mechanism, divalent cations present in the connate brine (water naturally present in the oil reservoir before any waterflooding has taken place) attract oil to the clay by forming a bridge across the thin film of water separating the oil and the clay, binding the negatively charged carboxylate

ions on the oil surface to the negatively charged exchange sites on the clay surface. Lager et al. assert that, as the concentration of divalent ions in the injected water is decreased, the ions attracting the oil to the clay migrate into the bulk, and are replaced by monovalent ions, allowing the release of oil. Additionally, they claim that the thin film of water between the oil and clay expands in the low salinity regime, due to electric double layer expansion, reducing the attraction of the oil to the clay surface, and thus assisting the release of oil.

Numerous experimental studies have been undertaken to distinguish between these different mechanisms. The majority of these are core-scale experiments, in which a sample of reservoir rock, a 'core', approximately $10\text{cm}\times4\text{cm}^2$, is water-flooded with brine [9–11, 15, 18, 27, 32, 33]. By studying the effects of different oil, rock, and brine compositions, these experiments provide a good understanding of the requirements for effective low salinity oil recovery.

By performing core-scale experiments, Lager et al. [15] observe that a greater oil recovery can be achieved without any increase in the number of fines produced, or any significant permeability alteration, and thus they assert that fines migration is unlikely to be the dominant mechanism. They also dispute the pH increase mechanism, as low salinity effects were observed in experiments in which the pH only showed a slight increase.

As an alternative to a core experiment, Berg et al. [3] demonstrate the weakening of the adhesion forces between oil droplets and a clay surface in the low salinity regime, by passing water over oil on a clay surface. They observe that the oil droplets lift from the clay surface as the salinity of the surrounding fluid reduces. These results support the MIE mechanism proposed by Lager et al. [15].

A key component in the MIE mechanism is the expansion of the thin water film between the oil and clay. Lee et al. [16] used Small Angle Neutron Scattering to measure the thickness of the film, h^*, for various salinities, and found that h^* varies from 0.9 nm to 1.3 nm as the salinity of the surrounding fluid varies. These results support the MIE mechanism by demonstrating the effect of the double layer expansion, and the weakening of adhesion forces at the oil-clay interface, as the salinity of the surrounding fluid is reduced.

Theoretical predictions for the thickness of the thin layer of water between the clay and the oil have been made based on a balance between capillary pressure and electro-osmotic forces [8, 12, 31]. These forces are derived from Derjaguin, Verwey, Landau, and Overbeek's (DVLO) theory of colloidal stability [6, 30], in which the disjoining pressure, Π, is taken to be the same as between two flat plates [2, 20, 24–26]. However, there does not appear to be a systematic derivation of the height at which the oil lies above the clay where the oil-water interface is treated as a free surface. Further, the expressions often stated for the film thickness are for static models [8, 12–14, 31]; however, as can be seen by studing the motion of bubbles through capillary tubes [4] (the Bretherton model), or by studying the spreading of droplets on surfaces [29] (Tanner's Law), the film thickness below a moving droplet is dependent on the velocity at which the droplet moves, hence these static models are of limited use when studying oil motion through a pore space.

A systematic derivation for the motion of a fluid through a prewetted capillary in the presence of a disjoining pressure is given by Egorov et al. [7]. However, this model does not include electrostatic effects due to ion exchange. On the other hand, Kuchin et al. [13, 14] study the profile of a capillary meniscus with the inclusion of electrostatic effects. However, in their model the meniscus is static, and so they do not consider Bretherton effects which will influence the motion of oil.

In this paper, we study the paradigm problem of the two-dimensional steady motion of a charged oil slug in a charged pore throat, where the surrounding water contains both monovalent and divalent ions. In Section 2, we present a mathematical model to describe the motion of the oil slug, which includes a simple model for the reactions occurring between the ions and the surfaces.

Then, in Section 3, we solve the model and derive an expression for the velocity, V, at which the oil slug moves given a pressure difference, P, along the length of the pore throat. We also consider the asymptotic limit in which P is much smaller than the disjoining pressure due to the charged surfaces.

In Section 4, we will solve the model numerically in the high salinity and low salinity regimes to determine the shape and the velocity of the oil slug. We will solve the model assuming that the ratio of P to the disjoining pressure is $\mathcal{O}(1)$, and we will compare the results with the asymptotic solution in the limit in which this term tends to zero.

Finally, in Chapter 5, we will draw together our findings and discuss their application. Our aim is to provide a simple, testable model for the effect of a low salinity injection.

2 Model Formulation

We wish to model the motion of an oil slug through a pore throat filled with saline water, subject to a constant pressure difference, P, across the ends of the pore. We suppose that the pore throat can be represented by a capillary tube of length L and height $2R$, and that at each end of the capillary there is a bulk region of water. We label the oil region by Ω_o, the surrounding water region by Ω_w, and the clay regions bounding either side of the capillary tube by Ω_c, as shown in Figure 1. We assume that there is a thin film of water separating the oil from the clay surface (due to electrostatic and viscous effects) along the upper and lower surfaces of the oil slug. The thickness of this water layer is unknown *a priori*; however, we assume that it is thin enough such that from a macroscopic perspective there appears to be contact between the oil and the clay. We denote the length of the oil droplet, measured from the apparent contact point of the rear meniscus, to the apparent contact point of the front meniscus, by L_o, and we assume that $L_o = \mathcal{O}(L)$. Taking the origin of our coordinate system to be the lower left corner of the tube, we suppose that the upstream apparent contact point has horizontal coordinate x_c, with the positions of the front and rear menisci being x_f and x_r, as shown in Figure 2.

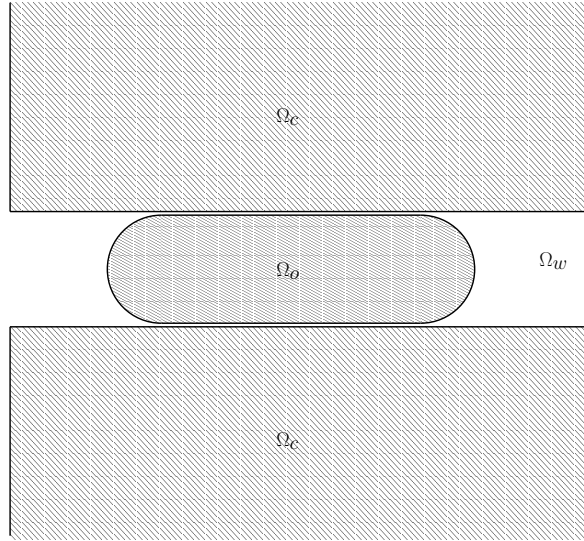In order to model the effect of the salinity of the water on the motion of

Figure 1: Schematic diagram of the motion of an oil slug through a capillary between two bulk phases of water.

the oil slug, we assume that the water phase contains solvated positively and negatively charged ions, with the concentrations of the monovalent and divalent species being $c^{\pm}$ and $c^{2\pm}$ respectively. In order to model ion exchange mechanisms on the capillary wall, and on the oil-water interface, we assume that these surfaces contain a number of negatively charged exchange sites at which reactions are allowed to occur. Using symmetry, we consider only the lower half of the capillary tube, that is, the region $z < R$.

2.1 Governing Equations

We model the oil and water using the Navier-Stokes equations. Due to the presence of the ions, the net charge density is $q(c^+ - c^- + 2c^{2+} - 2c^{2-})$ in the water phase, where q is the (absolute) charge of an electron. Hence, the electric field, $\nabla\phi$, induces a force on the water, and we have to include this body force in the equations for the water phase. Thus we write

$$\nabla \cdot \mathbf{u}_w = 0, \qquad\qquad \text{in } \Omega_w, \quad (1)$$

$$\rho_w \frac{D\mathbf{u}_w}{Dt} = -\nabla p_w + \mu_w \nabla^2 \mathbf{u}_w - q(c^+ - c^- + 2c^{2+} - 2c^{2-})\nabla\phi, \qquad \text{in } \Omega_w, \quad (2)$$

$$\nabla \cdot \mathbf{u}_o = 0, \qquad\qquad \text{in } \Omega_o, \quad (3)$$

$$\rho_o \frac{D\mathbf{u}_o}{Dt} = -\nabla p_o + \mu_o \nabla^2 \mathbf{u}_o, \qquad\qquad \text{in } \Omega_o, \quad (4)$$

where $\mathbf{u}_o = (u_o, w_o)$ is the velocity in the water phase, $\mathbf{u}_w = (u_w, w_w)$ is the velocity in the oil phase, p_w is the pressure in the water phase, p_o is the pressure in the oil phase, ρ_w is the density of the water, ρ_o is the density of the oil, μ_w is the viscosity of the water, μ_o, is the viscosity of the oil, and ϕ is the electric potential.
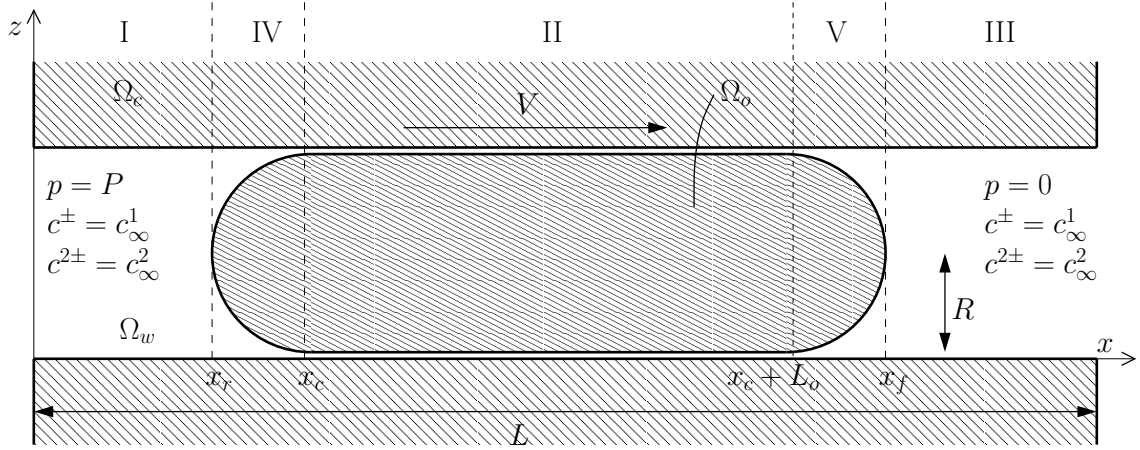
4

Figure 2: Schematic diagram of the macroscopic capillary problem. The thickness of the water layer below the oil slug has been exaggerated for illustrative purposes.

The ion concentrations are governed by the Nernst-Planck (Drift-Diffusion) equations,

$$\frac{\mathrm{D}c^\pm}{\mathrm{D}t} = D^\pm \nabla \cdot \left(\nabla c^\pm \mp \frac{q}{k_B T} c^\pm \nabla \phi \right), \qquad \text{in } \Omega_w, \qquad (5)$$

$$\frac{\mathrm{D}c^{2\pm}}{\mathrm{D}t} = D^{2\pm} \nabla \cdot \left(\nabla c^{2\pm} \mp \frac{2q}{k_B T} c^{2\pm} \nabla \phi \right), \qquad \text{in } \Omega_w, \qquad (6)$$

where $D^\pm$, $D^{2\pm}$, k_B, and T denote the diffusive coefficients of the monovalent and divalent ions, Boltzmann's constant, and the temperature, respectively. These are coupled to Poisson's equation, which determines the electric potential for a given charge distribution, which reads

$$\nabla^2 \phi = \begin{cases} \frac{q}{\varepsilon_w}(c^+ - c^- + 2c^{2+} - 2c^{2-}) & \text{in } \Omega_w, \\ 0 & \text{in } \Omega_o \cup \Omega_c, \end{cases} \qquad (7)$$

where ε_w is the permittivity of the water phase. Note that although we only need to solve the fluid equations inside the capillary, we need to solve Poisson's equation everywhere to determine ϕ.

2.2 Boundary Conditions

We set the concentrations of the monovalent and divalent ions to be c_∞^1 and c_∞^2, respectively, at each end of the tube. We suppose that there is no potential drop across the tube, so that $\phi(0) = \phi(L)$, which we may take to be zero without loss of generality. These boundary conditions read

$$p_w = P, \qquad \qquad \text{at } x = 0, \qquad (8)$$

$$p_w = 0, \qquad \qquad \text{at } x = L, \qquad (9)$$

$$c^\pm = c_\infty^1, \qquad c^{2\pm} = c_\infty^2, \qquad \phi = 0, \qquad \text{at } x = 0, L. \qquad (10)$$

5

We restrict our attention to the lower half of the capillary by imposing symmetry conditions on the surface $z = R$,

$$\frac{\partial u_w}{\partial z} = \frac{\partial u_o}{\partial z} = w_w = w_o = \frac{\partial p_w}{\partial z} = \frac{\partial p_o}{\partial z} = \frac{\partial c^{\pm}}{\partial z} = \frac{\partial c^{2\pm}}{\partial z} = \frac{\partial \phi}{\partial z} = 0. \qquad (11)$$

One of the advantages of considering only the lower half plane is that the oil-water interface becomes a single valued function in x. We denote this boundary by $z = h(x, t)$. On the capillary wall we impose the zero slip condition,

$$\mathbf{u}_w = 0, \qquad \text{at } z = 0, \qquad (12)$$

and on $z = h$ we impose continuity of velocity across the interface, the kinematic condition, and a balance of normal and tangential stresses. These conditions read

$$\mathbf{u}_w = \mathbf{u}_o, \qquad\qquad \text{at } z = h, \qquad (14)$$

$$h_t = w_w - u_w h_x, \qquad\qquad \text{at } z = h, \qquad (15)$$

$$\mathbf{n} \cdot \mathbf{T}_w \cdot \mathbf{t} = \mathbf{n} \cdot \mathbf{T}_o \cdot \mathbf{t}, \qquad\qquad \text{at } z = h, \qquad (16)$$
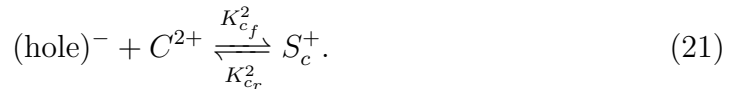
$$\mathbf{n} \cdot \mathbf{T}_w \cdot \mathbf{n} = \mathbf{n} \cdot \mathbf{T}_o \cdot \mathbf{n} + \frac{\gamma h_{xx}}{(1 + h_x^2)^{3/2}}, \qquad\qquad \text{at } z = h, \qquad (17)$$

where $\mathbf{n}$ and $\mathbf{t}$ are the normal and tangential vectors to the surface, respectively, and γ is the surface tension of the oil-water interface. We let $\mathbf{T}_w$ and $\mathbf{T}_o$ denote the stress tensors for the water and oil respectively, given by

$$\mathbf{T}_w = -p_w \mathbf{I} + \mu_w \left[\nabla \mathbf{u}_w + (\nabla \mathbf{u}_w)^T \right] + \varepsilon_w (\nabla \phi)(\nabla \phi)^T - \frac{\varepsilon_w}{2} |\nabla \phi|^2 \mathbf{I}, \qquad (18)$$

$$\mathbf{T}_o = -p_o \mathbf{I} + \mu_o \left[\nabla \mathbf{u}_o + (\nabla \mathbf{u}_o)^T \right]. \qquad (19)$$

To determine the boundary conditions for the ion concentrations, we need to consider the reactions occuring at the clay-water and oil-water interfaces. We model the reactions occuring at the clay-water interface by supposing that there are a number of negatively charged exchange sites on the clay surface which can either be occupied by a monovalent cation to create a neutrally charged site, a divalent cation to create a positively charged site, or remain unoccupied. We let C^+ and C^{2+} denote monovalent and divalent cations, and S_c and S_c^+ denote sites on the surface occupied by monovalent and divalent cations respectively. The subscript c denotes 'clay'. We suppose the following reactions[1] occur on the surface,

$$(\text{hole})^- + C^+ \underset{K_{c_r}^1}{\overset{K_{c_f}^1}{\rightleftharpoons}} S_c, \qquad (20)$$

$$(\text{hole})^- + C^{2+} \underset{K_{c_r}^2}{\overset{K_{c_f}^2}{\rightleftharpoons}} S_c^+. \qquad (21)$$

_____

[1]Note that, in order to model the effects of different reaction processes, such as pH variation, we can replace equations (20) and (21) and apply the same methodology.

The first equation describes the adsorption of monovalent ions to create neutrally charged sites, and the second describes the adsorption of divalent ions to create positively charged sites. The rate parameters $K_{c_f}^i$ and $K_{c_r}^i$ are the forward and reverse reaction rates, repectively, for the reaction involving the ion of valence i. We let s_c and s_c^+ denote the concentrations of adsorbed monovalent and divalent cations respectively, and let s_c^* be the saturation concentration, which we assume is constant along the capillary wall. Using the principle of mass action, we obtain the following equations on the capillary surface, $\partial \Omega_c$,

$$\frac{\partial s_c}{\partial t} = K_{c_f}^1 c^+ (s_c^* - s_c - s_c^+) - K_{c_r}^1 s_c, \tag{22}$$

$$\frac{\partial s_c^+}{\partial t} = K_{c_f}^2 c^{2+} (s_c^* - s_c - s_c^+) - K_{c_r}^2 s_c^+. \tag{23}$$

Balancing the flux of ions to the surface with the rate at which ions react with the surface sites yields the boundary conditions

$$D^\pm \left(\frac{\partial c^+}{\partial z} - \frac{q}{k_B T} c^+ \frac{\partial \phi}{\partial z} \right) = \frac{\partial s_c}{\partial t}, \tag{24}$$

$$D^{2\pm} \left(\frac{\partial c^{2+}}{\partial z} - \frac{2q}{k_B T} c^{2+} \frac{\partial \phi}{\partial z} \right) = \frac{\partial s_c^+}{\partial t}, \tag{25}$$

on $z = 0$. By assuming that similar reactions occur on the oil-water interface, with carboxylic acid groups being represented by negatively charged exchange sites, we also have the following set of boundary conditions on the surface of the oil, $z = h$,

$$\frac{\mathrm{D} s_o}{\mathrm{D} t} = K_{o_f}^1 c^+ (s_o^* - s_o - s_o^+) - K_{o_r}^1 s_o, \tag{26}$$

$$\frac{\mathrm{D} s_o^+}{\mathrm{D} t} = K_{o_f}^2 c^{2+} (s_o^* - s_o - s_o^+) - K_{o_r}^2 s_o^+, \tag{27}$$

$$D^\pm \mathbf{n} \cdot \left(\nabla c^+ - \frac{q}{k_B T} c^+ \nabla \phi \right) = \frac{\mathrm{D} s_o}{\mathrm{D} t}, \tag{28}$$

$$D^{2\pm} \mathbf{n} \cdot \left(\nabla c^{2+} - \frac{2q}{k_B T} c^{2+} \nabla \phi \right) = \frac{\mathrm{D} s_o^+}{\mathrm{D} t}, \tag{29}$$

where the subscript o denotes 'oil'. We assume that s_o^* is constant along the oil-water interface. As the negatively charged ions do not react with the surface, we have the zero flux conditions

$$\mathbf{n} \cdot \left(\nabla c^- + \frac{q}{k_B T} c^- \nabla \phi \right) = 0, \tag{30}$$

$$\mathbf{n} \cdot \left(\nabla c^{2-} + \frac{2q}{k_B T} c^{2-} \nabla \phi \right) = 0, \tag{31}$$

on $z = 0, h$.

Equations (22) - (31) are the boundary conditions for the ion concentrations at the clay-water interface, and the oil-water interface. As the surface concentration of negatively charged, unoccupied sites is given by $s_c^* - s_c - s_c^+$ on the clay-water

interface, and $s_o^* - s_o - s_o^+$ on the oil-water interface, respectively, the surface charge densities are given by $\sigma_c = q(2s_c^+ + s_c - s_c^*)$, and $\sigma_o = q(2s_o^+ + s_o - s_o^*)$, for the clay and oil surfaces respectively.

Due to the charged surfaces, there is a discontinuity in the electric field across the clay-water and oil-water interfaces, given by the difference in the ratio of the surface charge density to the permittivity. We also impose that the electric field is zero at infinity, since we assume that the system is globally neutral. These conditions read

$$[\varepsilon \phi_z]_-^+ = \sigma_c \qquad\qquad \text{at } z = 0, \tag{32}$$

$$[\varepsilon \mathbf{n} \cdot \nabla \phi]_-^+ = \sigma_o \qquad\qquad \text{at } z = h, \tag{33}$$

$$\nabla \phi \to 0 \qquad\qquad \text{as } x^2 + z^2 \to \infty, \tag{34}$$

where the permittivity is given by $\varepsilon = \varepsilon_w$ in the water phase, $\varepsilon = \varepsilon_o$ in the oil phase, and $\varepsilon = \varepsilon_c$ in the clay phase.

Finally, we also assume that the electric potential is continuous across these interfaces,

$$[\phi]_-^+ = 0 \qquad \text{at } z = 0, h. \tag{35}$$

2.3   Non-dimensionalisation

We non-dimensionalise the problem using the following scalings,

$$x = L\hat{x}, \qquad z = R\hat{z}, \qquad h = R\hat{h}, \tag{36a,b,c}$$

$$u_w = U\hat{u}_w, \qquad u_o = U\hat{u}_o, \qquad w_w = \epsilon_1 U\hat{w}_w, \qquad w_o = \epsilon_1 U\hat{w}_o, \tag{37a,b,c,d}$$

$$p_w = P\hat{p}_w, \qquad p_o = P\hat{p}_o, \qquad t = \frac{L}{U}\hat{t}, \tag{38a,b}$$

$$c^\pm = c_\infty^1 \hat{c}^\pm, \qquad c^{2\pm} = c_\infty^2 \hat{c}^{2\pm}, \qquad \phi = \frac{qs_c^* R}{\varepsilon_w}\hat{\phi}, \qquad \varepsilon = \varepsilon_w \hat{\varepsilon} \tag{39a,b,c,d}$$

$$s_c = s_c^* \hat{s}_c, \qquad s_c^+ = s_c^* \hat{s}_c^+, \qquad s_o = s_o^* \hat{s}_o, \qquad s_o^+ = s_o^* \hat{s}_o^+, \tag{40a,b,c,d}$$

where we pick $U = \frac{PR^2}{\mu_w L}$ in order to get a balance in (2), and $\epsilon_1 = R/L$ is the aspect ratio of the capillary tube.

After substituting in these variables, and dropping the hats, the dimensionless equations read

$$\epsilon_1^2 \mathrm{Re} \frac{\mathrm{D}u_w}{\mathrm{D}t} = -p_{wx} + \left(\epsilon_1^2 u_{wxx} + u_{wzz}\right)$$
$$- \frac{1}{\delta P^*}(c^+ - c^- + 2c^* c^{2+} - 2c^* c^{2-})\phi_x, \qquad \text{in } \Omega_w, \quad (41)$$

$$\epsilon_1^4 \mathrm{Re} \frac{\mathrm{D}w_w}{\mathrm{D}t} = -p_{wz} + \epsilon_1^2(\epsilon_1^2 w_{wxx} + w_{wzz})$$
$$- \frac{1}{\delta P^*}(c^+ - c^- + 2c^* c^{2+} - 2c^* c^{2-})\phi_z, \qquad \text{in } \Omega_w, \quad (42)$$

$$u_{wx} + w_{wz} = 0, \qquad \text{in } \Omega_w, \quad (43)$$

$$\epsilon_1^2 \rho^* \mathrm{Re} \frac{\mathrm{D}u_o}{\mathrm{D}t} = -p_{ox} + \mu^* \left(\epsilon_1^2 u_{oxx} + u_{ozz}\right), \qquad \text{in } \Omega_o, \quad (44)$$

$$\epsilon_1^4 \rho^* \mathrm{Re} \frac{\mathrm{D}w_o}{\mathrm{D}t} = -p_{oz} + \epsilon_1^2 \mu^* \left(\epsilon_1^2 w_{oxx} + w_{ozz}\right), \qquad \text{in } \Omega_o, \quad (45)$$

$$u_{ox} + w_{oz} = 0, \qquad \text{in } \Omega_o, \quad (46)$$

$$\epsilon_1^2 \mathrm{Pe}^{\pm} \frac{\mathrm{D}c^{\pm}}{\mathrm{D}t} = \epsilon_1^2 \left(c_x^{\pm} \mp \xi c^{\pm} \phi_x\right)_x + \left(c_z^{\pm} \mp \xi c^{\pm} \phi_z\right)_z, \qquad \text{in } \Omega_w \quad (47)$$

$$\epsilon_1^2 \mathrm{Pe}^{2\pm} \frac{\mathrm{D}c^{2\pm}}{\mathrm{D}t} = \epsilon_1^2 \left(c_x^{2\pm} \mp 2\xi c^{2\pm} \phi_x\right)_x + \left(c_z^{2\pm} \mp 2\xi c^{2\pm} \phi_z\right)_z, \qquad \text{in } \Omega_w, \quad (48)$$

$$\delta \left(\epsilon_1^2 \phi_{xx} + \phi_{zz}\right) = \begin{cases} c^+ - c^- + 2c^* c^{2+} - 2c^* c^{2-} & \text{in } \Omega_w, \\ 0 & \text{in } \Omega_o \cup \Omega_c. \end{cases} \qquad (49)$$

$$\varepsilon = 1 \text{ in } \Omega_w, \qquad \varepsilon = \varepsilon_1 \text{ in } \Omega_o, \qquad \varepsilon = \varepsilon_2 \text{ in } \Omega_c, \qquad (50)$$

The dimensionless parameters in the above equations are as follows; $\mathrm{Re} = \rho_w P R^2 / \mu_w^2$ is the Reynolds number, $\mathrm{Pe}^{\pm,2\pm} = P R^2 / D^{\pm,2\pm} \mu_w$ are the Peclet numbers for the different ionic species, $\delta = s_c^*/c_\infty^1 R$ is the ratio of the adsorption depth to the radius of the capillary, $P^* = \varepsilon_w P / q^2 s_c^{*2}$ is the ratio of the pressure drop across the capillary to the electrostatic pressure due to the charged surfaces, $\xi = q^2 s_c^* R / \varepsilon_w k_B T$ is the ratio of the potential due to the charged surfaces to the thermal voltage, $\rho^* = \rho_o/\rho_w$ is the ratio of the density of the oil to the density of the water, $\mu^* = \mu_o/\mu_w$ is the ratio of the viscosity of the oil to the viscosity of the water, and $c^* = c_\infty^2 / c_\infty^1$ is the ratio of the bulk concentration of divalent ions to the bulk concentration of monovalent ions. The dimensionless permittivity is $\varepsilon_1 = \varepsilon_o/\varepsilon_w$ in the oil phase, and $\varepsilon_2 = \varepsilon_c/\varepsilon_w$ in the clay phase.

These equations are subject to the boundary conditions

$$p_w = 1, \qquad c^{\pm,2\pm} = 1, \qquad \phi = 0, \qquad\qquad \text{at } x = 0, \qquad (51)$$

$$p_w = 0, \qquad c^{\pm,2\pm} = 1, \qquad \phi = 0, \qquad\qquad \text{at } x = 1, \qquad (52)$$

$$\left.\begin{aligned}
& \mathbf{u}_w = 0, \qquad [\varepsilon\phi_z]_-^+ = 2s_c^+ + s_c - 1, \qquad [\phi]_-^+ = 0, \\
& \Lambda_c^1 \frac{\partial s_c}{\partial t} = \mathcal{K}_c^1 c^+ (1 - s_c - s_c^+) - s_c, \\
& \Lambda_c^2 \frac{\partial s_c^+}{\partial t} = \mathcal{K}_c^2 c^{2+} (1 - s_c - s_c^+) - s_c^+, \\
& c_z^+ - \xi c^+ \phi_z = \epsilon_1^2 \delta \mathrm{Pe}^+ \frac{\partial s_c}{\partial t}, \qquad c_z^- + \xi c^- \phi_z = 0, \\
& c_z^{2+} - 2\xi c^{2+}\phi_z = \frac{\epsilon_1^2 \delta \mathrm{Pe}^{2+}}{c^*} \frac{\partial s_c^+}{\partial t}, \qquad c_z^{2-} + 2\xi c^{2-}\phi_z = 0,
\end{aligned}\right\} \quad \text{at } z = 0, \quad (53)$$

$$\left.\begin{aligned}
& \mathbf{u}_w = \mathbf{u}_o \qquad h_t = w_w - u_w h_x, \\
& \Lambda_o^1 \frac{\mathrm{D}s_o}{\mathrm{D}t} = \mathcal{K}_o^1 c^+ (1 - s_o - s_o^+) - s_o, \\
& \Lambda_o^2 \frac{\mathrm{D}s_o^+}{\mathrm{D}t} = \mathcal{K}_o^2 c^{2+} (1 - s_o - s_o^+) - s_o^+, \\
& c_z^+ - \xi c^+ \phi_z - \epsilon_1^2 h_x \left(c_x^+ - \xi c^+ \phi_x\right) = \epsilon_1^2 \delta \mathrm{Pe}^+ s^* \frac{\mathrm{D}s_o}{\mathrm{D}t}, \\
& c_z^{2+} - 2\xi c^{2+}\phi_z - \epsilon_1^2 h_x \left(c_x^{2+} - 2\xi c^{2+}\phi_x\right) = \frac{\epsilon_1^2 \delta \mathrm{Pe}^{2+} s^*}{c^*} \frac{\mathrm{D}s_o^+}{\mathrm{D}t}, \\
& c_z^- + \xi c^- \phi_z - \epsilon_1^2 h_x \left(c_x^- + \xi c^- \phi_x\right) = 0, \\
& c_z^{2-} + 2\xi c^{2-}\phi_z - \epsilon_1^2 h_x \left(c_x^{2-} + 2\xi c^{2-}\phi_x\right) = 0, \\
& \frac{1}{(1+\epsilon_1^2 h_x^2)^{1/2}} \left[\varepsilon \left(\phi_z - \epsilon_1^2 h_x \phi_x\right)\right]_-^+ = s^*(2s_o^+ + s_o - 1), \\
& [\phi]_-^+ = 0,
\end{aligned}\right\} \quad \text{at } z = h, \quad (54)$$

$$u_{wz} = u_{oz} = w_w = w_o = p_{wz} = p_{oz} = c_z^\pm = c_z^{2\pm} = \phi_z = 0, \qquad \text{at } z = 1, \quad (55)$$

$$\nabla\phi \to \mathbf{0}, \qquad\qquad \text{as } x^2 + z^2 \to \infty. \quad (56)$$

Substituting in the expressions for the stress tensors, (18) and (19), the boundary conditions (16) and (17) read

$$\mu^* \left[(u_{oz} + \epsilon_1 w_{oz})(1 - \epsilon_1^2 h_x^2) + 2\epsilon_1^2 h_x(w_{oz} - u_{ox})\right] = (u_{wz} + \epsilon_1 w_{wz})(1 - \epsilon_1^2 h_x^2)$$
$$+ 2\epsilon_1^2 h_x(w_{wz} - u_{wx}) + \frac{\epsilon_1}{P^*} \left[h_x(\epsilon_1^2 \phi_x^2 - \phi_z^2) + (1 - \epsilon_1^2 h_x^2)\phi_x\phi_z\right]^-, \quad (57)$$

$$\epsilon_1^2 \mu^* \frac{[w_{oz} - h_x u_{oz} + \epsilon_1^2 h_x(h_x u_{ox} - w_{ox})]}{1 + \epsilon_1^2 h_x^2} = \epsilon_1^2 \frac{[w_{wz} - h_x u_{wz} + \epsilon_1^2 h_x(h_x u_{wx} - w_{wx})]}{1 + \epsilon_1^2 h_x^2}$$
$$+ \frac{1}{2}(p_o - p_w) - \frac{1}{P^*} \left[\frac{\epsilon_1^2 h_x \phi_x \phi_z}{1 + \epsilon_1^2 h_x^2} + \frac{1}{4}(\epsilon_1^2 \phi_x^2 - \phi_z^2)\right]^- - \frac{\Gamma h_{xx}}{4P^*(1 + \epsilon_1^2 h_x^2)^{3/2}}, \quad (58)$$

on $z = h$. The ratios of the timescales of the surface reactions to the timescale chosen for the non-dimensionalisation are given by $\Lambda_c^{1,2} = PR^2/\mu_w L^2 K_{cr}^{1,2}$ and $\Lambda_o^{1,2} = PR^2/\mu_w L^2 K_{or}^{1,2}$, the dimensionless dissociation constants are $\mathcal{K}_c^{1,2} = K_{cf}^{1,2} c_\infty^{1,2}/K_{cr}^{1,2}$ and $\mathcal{K}_o^{1,2} = K_{of}^{1,2} c_\infty^{1,2}/K_{or}^{1,2}$, the ratio of the surface tension forces to the electrostatic forces is $\Gamma = 2\gamma\varepsilon_w R/L^2 q^2 s_c^{*2}$ ($2\epsilon_1^3 P^*/\Gamma$ is the capillary number, with the chosen velocity scale), and $s^* = s_o^*/s_c^*$ is the ratio of the saturation concentration of the oil surface to the saturation concentration of the clay surface.

Austad et al. [1] performed experiments using brine with low salinity $c_\infty^1 \approx 1 \cdot 10^{25}$ m^{-3}, $c_\infty^2 \approx 3 \cdot 10^{24}$ m^{-3}, and high salinity $c_\infty^1 \approx 1 \cdot 10^{27}$ m^{-3}, $c_\infty^2 \approx 5.4 \cdot 10^{25}$ m^{-3}, hence we take these to be our low salinity and high salinity regimes, respectively. In a given sample of reservoir rock there will be a range of pore throat sizes. Nelson [23] studies the distribution of these throat sizes for various rocks, and for the purposes of this paper we assume $R = 10^{-6}$ m, which is typical for a sandstone reservoir. The grain size, and hence the length of a typical pore throat, is typically an order of magnitude larger, so we assume that $L = 10^{-5}$ m. For the oil viscosity, density, and interfacial tension, we use values determined for a range of oil samples by Buckley [5]. Typically, $\gamma \approx 0.02$ J m^{-2}, with some variation depending on pH. The viscosities of the oils used by Buckley ranged from $0.006 - 0.035$ kg m^{-1} s^{-1}, so we let $\mu_o = 0.01$ kg m^{-1} s^{-1}. The oil densities were in the range $840 - 900$ kg m^{-3}, so we let $\rho_o = 850$ kg m^{-3}. The viscosity of water is $8.9 \cdot 10^{-4}$ kg m^{-1} s^{-1}, and the density of water is 1000 kg m^{-3}. Flow rates in a reservoir are typically around 10^{-5} m s^{-1} (≈ 3 ft day^{-1}), so, using Poiseuille's law for flow through a cylinder, $\Delta P \sim 8\mu_w L V/R^2$, we find that the typical pressure difference across a pore throat is $P \approx 0.7$ N m^{-2}. Alternatively, we can estimate the pressure using Darcy's law $Q = K\Delta P/\mu L$. For $K = 100$ mD, we find that $\Delta P \approx 1$ N m^{-2}, agreeing with our previous estimation.

Lager et al. [15] studied core scale experiments at $102°$C, so we let $T = 375°$K, and hence by using $\varepsilon_w = \varepsilon_{wr}\varepsilon_0$, where $\varepsilon_{wr} \approx 56$ [19] and $\varepsilon_0 \approx 8.9 \cdot 10^{-12}$ C^{2}J^{-1} m^{-1} are the relative permittivity of water at $100°$C, and the permittivity of free space, respectively, we find that $\varepsilon_w \approx 5 \cdot 10^{-10}$ C^2 J^{-1} m^{-1}. We take $D^+ \approx 1.3 \cdot 10^{-9}$ m^2 s^{-1}, $D^- \approx 2 \cdot 10^{-9}$ m^2 s^{-1}, $D^{2+} \approx 7.9 \cdot 10^{-10}$ m^2 s^{-1}, and $D^{2-} \approx 1.1 \cdot 10^{-9}$ m^2 s^{-1}, as these are the mass diffusivities of sodium, chloride, sulfate, and calcium ions, respectively [28]. We use the standard values for $q \approx 1.6 \cdot 10^{-19}$ C and $k_B \approx 1.4 \cdot 10^{-23}$ J K^{-1}. Li and Xu [17] studied the surface charge densities for different clays for various values of the pH. For a binary system containing kaolinite, a typical surface charge has a range from approximately $-5 \cdot 10^{-4}$ to $5 \cdot 10^{-4}$ C m^{-2}. Hence, by supposing that $\sigma_c \approx q s_c^*$, we estimate $s_c^* \approx 10^{16}$ m^{-2}.

Using these values, we find that $\epsilon_1 \approx 0.1 \ll 1$. The Reynolds number is Re $\approx 8.8 \cdot 10^{-4} \ll 1$, hence we will neglect the inertial terms in the Navier-Stokes equations. The Peclet numbers are Pe$^+ \approx 0.61$, Pe$^- \approx 0.39$, Pe$^{2+} \approx 1$, Pe$^{2-} \approx 0.72$, hence we will assume that these are $\mathcal{O}(1)$. Note that the ions in the model (Na$^+$, Cl$^-$, Ca^{2+}) have radius $\approx 2 \cdot 10^{-10}$ m, hence the continuum assumption breaks down as we approach the high salinity regime. However, as we are mainly interested in the effects of low salinity water, we will assume that we can make this approximation. We also assume that the ions react instantaneously

at the surfaces, that is, we assume that $\Lambda_c^{1,2} \ll 1$ and $\Lambda_o^{1,2} \ll 1$.

We find that $\xi \approx 98$, and that, depending on the salinity, δ ranges from 10^{-3} to 10^{-5}, hence, $\delta \ll \xi^{-1} \ll 1$. In Section 3 we will derive an expression for σ_c as a function of $\mathcal{K}_c^{1,2}$, and hence, by using the range of values for σ_c given by Li and Xu [17], we will estimate the values of the dissociation constants. To find the values for these constants, and the saturation concentrations, more accurately, an experimental investigation would have to be undertaken; however, this is beyond the scope of this paper. Using the estimated value for s_c^*, we find that $\Gamma \approx 0.08$, and $P^* \approx 1.4 \cdot 10^{-4}$, and hence we will find the solution in the limit $P^* \to 0$. However, as there can be large variations in the permeability and pore sizes between different rocks, and even within the same type of rock, we will consider $P^* = \mathcal{O}(1)$ in order to accommodate the wide-ranging conditions found in oil reservoirs. See Appendix A for a table of values.

Neglecting terms proportional to ϵ_1, Re, $\Lambda_c^{1,2}$, and $\Lambda_o^{1,2}$, equations (41) - (58) read

$$\left. \begin{array}{c} u_{wzz} = p_{wx} + \dfrac{1}{\delta P^*}(c^+ - c^- + 2c^* c^{2+} - 2c^* c^{2-})\phi_x, \\[2mm] p_{wz} = -\dfrac{1}{\delta P^*}(c^+ - c^- + 2c^* c^{2+} - 2c^* c^{2-})\phi_z, \\[2mm] u_{wx} + w_{wz} = 0, \end{array} \right\} \quad \text{in } \Omega_w, \qquad (59)$$

$$\mu^* u_{ozz} = p_{ox}, \qquad p_{oz} = 0, \qquad u_{ox} + w_{oz} = 0, \qquad \text{in } \Omega_o, \qquad (60)$$

$$\left(c_z^\pm \mp \xi c^\pm \phi_z\right)_z = 0, \qquad \left(c_z^{2\pm} \mp 2\xi c^{2\pm} \phi_z\right)_z = 0, \qquad \text{in } \Omega_w, \qquad (61)$$

$$\delta \phi_{zz} = \begin{cases} c^+ - c^- + 2c^* c^{2+} - 2c^* c^{2-} & \text{in } \Omega_w, \\ 0 & \text{in } \Omega_o \cup \Omega_c, \end{cases} \qquad (62)$$

$$\varepsilon = 1 \text{ in } \Omega_w, \qquad\qquad \varepsilon = \varepsilon_1 \text{ in } \Omega_o, \qquad\qquad \varepsilon = \varepsilon_2 \text{ in } \Omega_c, \qquad (63)$$

subject to

$$p_w = 1, \qquad c^{\pm,2\pm} = 1, \qquad \phi = 0, \qquad\qquad \text{at } x = 0, \quad (64)$$

$$p_w = 0, \qquad c^{\pm,2\pm} = 1, \qquad \phi = 0, \qquad\qquad \text{at } x = 1, \quad (65)$$

$$\left.\begin{aligned}
\mathbf{u}_w = 0, \qquad [\varepsilon\phi_z]_-^+ = 2s_c^+ + s_c - 1, \qquad [\phi]_-^+ = 0, \\
\mathcal{K}_c^1 c^+ (1 - s_c - s_c^+) - s_c = 0, \\
\mathcal{K}_c^2 c^{2+} (1 - s_c - s_c^+) - s_c^+ = 0, \\
c_z^\pm \mp \xi c^\pm \phi_z = 0, \qquad c_z^{2\pm} \mp 2\xi c^{2\pm} \phi_z = 0,
\end{aligned}\right\} \qquad \text{at } z = 0, \quad (66)$$

$$\left.\begin{aligned}
\mathbf{u}_w = \mathbf{u}_o, \qquad [\varepsilon\phi_z]_-^+ = s^*(2s_o^+ + s_o - 1), \qquad [\phi]_-^+ = 0, \\
\mathcal{K}_o^1 c^+ (1 - s_o - s_o^+) - s_o = 0, \\
\mathcal{K}_o^2 c^{2+} (1 - s_o - s_o^+) - s_o^+ = 0, \\
c_z^\pm \mp \xi c^\pm \phi_z = 0, \qquad c_z^{2\pm} \mp 2\xi c^{2\pm} \phi_z = 0, \\
h_t = w_w - u_w h_x, \qquad \mu^* u_{oz} = u_{wz}, \\
p_w = p_o + \frac{1}{2P^*}\left[\phi_z^2\right]^- - \frac{\Gamma h_{xx}}{2P^*},
\end{aligned}\right\} \qquad \text{at } z = h, \quad (67)$$

$$u_{wz} = u_{oz} = w_w = w_o = p_{wz} = p_{oz} = c_z^\pm = c_z^{2\pm} = \phi_z = 0, \qquad \text{at } z = 1, \quad (68)$$

$$\nabla\phi \to \mathbf{0}, \qquad\qquad\qquad \text{as } x^2 + z^2 \to \infty. \quad (69)$$

In order to form a closed system, we require solvability conditions for $c^\pm, c^{2\pm}$, and ϕ. These are obtained by integrating (47) and (48) from $z = 0$ to $z = 1$, which, after imposing (66) and (67), read

$$\mathrm{Pe}^\pm \int_0^1 \frac{\mathrm{D}c^\pm}{\mathrm{D}t}\,\mathrm{d}z = \frac{\partial}{\partial x}\int_0^1 \frac{\partial c^\pm}{\partial x} \mp \xi c^\pm \frac{\partial \phi}{\partial x}\,\mathrm{d}z, \qquad\qquad \text{in } \Omega_w, \qquad (70)$$

$$\mathrm{Pe}^{2\pm} \int_0^1 \frac{\mathrm{D}c^{2\pm}}{\mathrm{D}t}\,\mathrm{d}z = \frac{\partial}{\partial x}\int_0^1 \frac{\partial c^{2\pm}}{\partial x} \mp 2\xi c^{2\pm} \frac{\partial \phi}{\partial x}\,\mathrm{d}z, \qquad\qquad \text{in } \Omega_w. \qquad (71)$$

3 Model Solution

In Section 3.1, we solve (61) and (62) subject to (64) - (71) to find expressions for ϕ and $c^{1,2\pm}$. In Section 3.2 we use these expressions to solve (59) and (60) subject to (64) - (69), to find the shape and the velocity of the oil slug.

3.1 The Electric Potential

3.1.1 In the oil phase

To find ϕ in the oil phase, Ω_o, we consider (62), which reads

$$\phi_{zz} = 0. \qquad (72)$$

Hence, imposing (68), we get that $\phi_z \equiv 0$ in the oil. To find $\phi(x,t)$ we will need to first solve for ϕ in the water phase, and then impose (67).

3.1.2 In the water phase

In the water phase, Ω_w, integrating (61) twice and applying (66) yields

$$c^{k\pm} = d^{k\pm}e^{\pm k\xi\phi}, \tag{73}$$

for some functions $d^{\pm,2\pm}(x,t)$, for $k = 1,2$. By substituting (73) into (62), (70), and (71), we find that

$$\delta\phi_{zz} = d^+e^{\xi\phi} - d^-e^{-\xi\phi} + 2c^*(d^{2+}e^{2\xi\phi} - d^{2-}e^{-2\xi\phi}), \tag{74}$$

$$\mathrm{Pe}^{k\pm}\left[\frac{\partial}{\partial t}\int_0^1 d^{k\pm}e^{\pm k\xi\phi}\mathrm{d}z + \int_0^1(\mathbf{u}_w\cdot\nabla)d^{k\pm}e^{\pm k\xi\phi}\,\mathrm{d}z\right] = \left[\int_0^1 d_x^{k\pm}e^{\pm k\xi\phi}\mathrm{d}z\right]_x. \tag{75}$$

We expand in powers of δ to find that at leading order, $\phi \sim \phi_0 + \mathcal{O}(\delta)$ and $d^{\pm,2\pm} \sim d_0^{\pm,2\pm} + \mathcal{O}(\delta)$ satisfy

$$d_0^+e^{\xi\phi_0} - d_0^-e^{-\xi\phi_0} + 2c^*(d_0^{2+}e^{2\xi\phi_0} - d_0^{2-}e^{-2\xi\phi_0}) = 0. \tag{76}$$

It follows from (76) that $\phi_0 = \phi_0(x,t)$, and therefore (75) reads

$$\mathrm{Pe}^{k\pm}\left[(d_0^{k\pm}e^{\pm k\xi\phi_0})_t + (d_0^{k\pm}e^{\pm k\xi\phi_0})_x\int_0^1 u_w\,\mathrm{d}z\right] = (d_{0_x}^{k\pm}e^{\pm k\xi\phi_0})_x. \tag{77}$$

We observe that (77) admits constant solutions, and thus, by imposing (64) and (65), we find that $\phi_0 \equiv 0$, $d_0^{\pm,2\pm} \equiv 1$. By matching terms in (74) and (75) at higher orders and, we find that $\phi_i \equiv 0$, $d_i^{\pm,2\pm} \equiv 0$ for $i \geq 1$; hence, $\phi \equiv 0$, $d^{\pm,2\pm} \equiv 1$.

However, after imposing (66) and solving $\phi_{zz} = 0$ in the clay phase, this leads to ϕ_z becoming unbounded as $z \to -\infty$, which contradicts (69). Hence, there are boundary layers at the capillary wall, and at the oil-water interface, of size ϵ_2 (to be determined).

To look near the capillary wall, we define the rescaling $z = \epsilon_2 Z$. As we expect the thickness of the wetting film to be partly determined by the electrostatic forces occurring between the two charged surfaces, we require $h^* = \mathcal{O}(\epsilon_2)$. Otherwise, there is a bulk region between the surfaces in which $\phi = 0$, and therefore there is no interaction between the two surfaces. Hence, we define the rescaling $h = \epsilon_2 H$. From (66) and (67), we observe that the rescaling $\phi = \epsilon_2 \Phi$ is required to balance the terms in the boundary conditions. Substituting $d^{\pm,2\pm} = 1$ into (74), and expanding the resulting equation in terms of ϵ_2 (assuming that $\epsilon_2\xi \ll 1$) yields

$$\frac{\delta}{\epsilon_2^2}\Phi_{ZZ} = 2(1+4c^*)\xi\Phi + \mathcal{O}(\epsilon_2). \tag{78}$$

To balance the leading-order terms in (78) we find that $\epsilon_2 = \left(\frac{\delta}{2\xi^2(1+4c^*)}\right)^{1/2} = \lambda/R$, where $\lambda = \left(\frac{\varepsilon_w k_B T}{2(c_\infty^1 + 4c_\infty^2)q^2}\right)^{1/2}$ is the Debye length. Note that with this choice of ϵ_2, the assumption we made, that $\epsilon_2\xi \ll 1$, holds, and therefore the asymptotic analysis is consistent.

The equations governing the potential in the boundary layer at leading order in ϵ_2 read

$$\Phi_{ZZ} = \Phi, \tag{79}$$

subject to

$$[\Phi]_-^+ = 0, \quad [\varepsilon \Phi_Z]_-^+ = 2s_{c0}^+ + s_{c0} - 1, \qquad \text{at } Z = 0, \tag{80}$$

$$[\Phi]_-^+ = 0, \quad \Phi_Z|^- = -s^*(2s_{o0}^+ + s_{o0} - 1), \quad \text{at } Z = H, \quad x_r^* < x < x_f^* \tag{81}$$

$$\Phi_Z \to 0, \qquad \text{as } Z \to \infty, \quad \begin{cases} 0 < x < x_r^*, \\ x_f^* < x < 1, \end{cases} \tag{82}$$

$$\Phi = 0, \qquad \text{at } x = 0, 1, \tag{83}$$

where $x_f^* = x_f/L$ and $x_r^* = x_r/L$ are the dimensionless positions of the front and rear of the menisci of the oil slug, respectively. Equation (82) is the matching condition required to ensure that the potential in the boundary layer, Φ, matches with the outer solution, $\phi_0 = 0$. Note that we have used the fact that $\phi_z = 0$ in the oil phase in deriving (81).

To solve (79) - (83) for Φ in the boundary layer, we need to find expressions for s_{c0}, s_{c0}^+, s_{o0}, and s_{o0}^+. By substituting $c_0^{\pm,2\pm} = 1$ into (66) and (67), we get that

$$s_{c0} = \frac{\mathcal{K}_c^1}{1 + \mathcal{K}_c^1 + \mathcal{K}_c^2}, \qquad s_{c0}^+ = \frac{\mathcal{K}_c^2}{1 + \mathcal{K}_c^1 + \mathcal{K}_c^2}, \tag{84}$$

$$s_{o0} = \frac{\mathcal{K}_o^1}{1 + \mathcal{K}_o^1 + \mathcal{K}_o^2}, \qquad s_{o0}^+ = \frac{\mathcal{K}_o^2}{1 + \mathcal{K}_o^1 + \mathcal{K}_o^2}. \tag{85}$$

Using the relations for the surface charge densities, $\sigma_c = 2s_c^+ + s_c - 1$, and $\sigma_o = 2s_o^+ + s_o - 1$, we find that

$$\sigma_{c0} = \frac{\mathcal{K}_c^2 - 1}{1 + \mathcal{K}_c^1 + \mathcal{K}_c^2}, \qquad \sigma_{o0} = \frac{\mathcal{K}_o^2 - 1}{1 + \mathcal{K}_o^1 + \mathcal{K}_o^2}. \tag{86}$$

Note that σ_{c0} and σ_{o0} are constant along the capillary surface, and oil-water interface, respectively, as at leading order the ion concentrations are constant.

Recalling that $\mathcal{K}_c^{1,2} = K_{c_f}^{1,2} c^{1,2+}/K_{c_r}^{1,2}$, we find that in order for the surface charge densities to agree with the values found by Li and Xu [17] as the bulk salinity varies, appropriate values for the dimensional dissociation constants are $K_{c_f}^1/K_{c_r}^1 \sim 3 \cdot 10^{-28}$ m^3, and $K_{c_f}^2/K_{c_r}^2 \sim 4.1 \cdot 10^{-25}$ m^3. In order to study the effect of having different materials on the two surfaces, we suppose that the dissociation constants are different on the two surfaces.

The water phase can be split into five regions, shown in Figure 2; the bulk region of water to the left of the oil slug (region I), the thin layer of water separating the oil from the capillary walls (region II), the bulk region of water to the right of the oil slug (region III), and the meniscus regions at each end of the oil slug (regions IV and V). For $0 < x < x_r^*$ (region I), Φ satisfies (79) subject to (82), which can be solved to find

$$\Phi = -A e^{-Z}, \tag{87}$$

where $A(x)$ is defined for $0 < x < x_f^*$. Similarly, solving (79) subject to (82) for $x_f^* < x < 1$ (region III) yields the same expression, with $A(x)$ defined for $x_f^* < x < 1$.

In the thin water layer between the oil and the clay surface, $x_c^* < x < x_c^* + L_o^*$ (region II), where $x_{c*} = x_c/L$ and $L_o^* = L_o/L$ are the dimensionless position of the apparent contant point and length of the oil slug respectively, due to the choice of scaling for the thickness of the layer, the clay-water and oil-water boundary layers overlap. Hence, instead of a far field condition, Φ satisfies (79) subject to (81). We solve this system to find

$$\Phi = A \sinh Z - \frac{A \cosh H + s^* \sigma_{o0}}{\sinh H} \cosh Z, \tag{88}$$

for some function $A(x)$ defined for $x_c^* < x < x_c^* + L_o^*$.

Note that exactly the same analysis applies in regions IV and V as in region II, yielding the same expression for Φ, (88). In region IV, as $x \to x_c^*$ the solution trivially matches with the solution in region II, and as $x \to x_r^*$, we find that $H \to \infty$, hence $\Phi \to -A e^{-Z}$ which matches the solution in region I. Similarly, region V matches regions II and III.

3.1.3 In the clay phase

In the clay phase, Ω_c, the leading order potential satisfies

$$\phi_{zz} = 0, \tag{89}$$

subject to

$$\frac{1}{\epsilon_2} \phi := \begin{cases} -A & x < x_r^*, \\ -\frac{A \cosh (h/\epsilon_2) + s^* \sigma_{o0}}{\sinh (h/\epsilon_2)} & x_r^* < x < x_f^*, \\ -A & x > x_f^*, \end{cases} \qquad z = 0, \tag{90}$$

$$\varepsilon_2 \phi_z = A - \sigma_{c0}, \qquad z = 0. \tag{91}$$

From (69), we have that ϕ is bounded, and by integrating (89) we find that $\phi_z = 0$. Hence, by imposing (91), we see that $A \equiv \sigma_{c0}$.

Thus, we use this result to determine the potential in the water phase, namely

$$\Phi = \begin{cases} \sigma_{c0} e^{-Z} & \text{in I, III}, \\ \sigma_{c0} \sinh Z - \frac{\sigma_{c0} \cosh H + s^* \sigma_{o0}}{\sinh H} \cosh Z, & \text{in II, IV, V}. \end{cases} \tag{92}$$

Having found an expression for the electric potential in the water phase, we can now solve Stokes' equations for the fluid (59) and (60) by substituting (92) into the expression for the body force. Hence, we are now in a position to find the velocity profile of the fluids, $\mathbf{u_w}$ and $\mathbf{u}_o$, and consequently the speed at which the oil slug moves through the capillary.
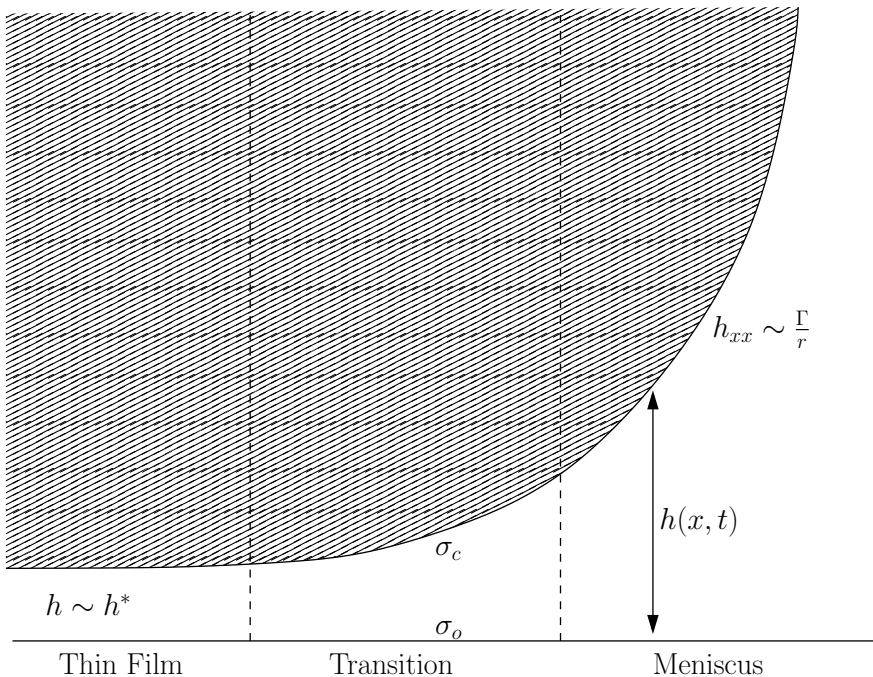
Figure 3: Schematic diagram of the three regions at the front meniscus.

3.2 The Fluid Velocity

As the shape of the oil slug is unknown a priori, it must be found as part of the solution. We will solve for the profile of the oil-water interface at the front and rear (downstream and upstream) ends of the oil slug separately, noting that the shape of the oil slug is different at each end due to the motion of the fluids in the capillary. We will first find the shape of the front end, assuming that the oil-water interface can be split into three distinct regions, shown in Figure 3. These are; (i) a flat region with constant thickness, h^* (to be determined), along the base of the oil slug, in which the capillary forces balance the electrostatic forces, (ii) a meniscus region with constant curvature, r^+ (to be determined), in which the capillary forces balance the surface tension forces, and (iii) a transition region matching regions (i) and (ii), in which the capillary forces are balanced by the electrostatic forces, and the surface tension forces.

We study the neighbourhood of the point where, from the macroscopic perspective, there appears to be a three phase contact (i.e. near $x = x_c + L_o$). We examine how the region of constant thickness matches with the region of constant curvature, and hence we will determine h^* and r^+. Once we have found the shape of the front end of the oil slug, we will use the transformation $V \mapsto -V$, where V is the velocity of the oil slug, in order to find the shape of the rear end, using the fact that the front end advances at the same speed that the rear end recedes.

3.2.1 Shape of the oil-water interface

In order to balance the hydrostatic, electrostatic, and surface tension forces in (59), (60), (66), and (67), we define the rescalings $x - (x_c^* + L_o^*) = \epsilon_2^{1/2} \bar{X}$, $z = \epsilon_2 Z$,

17

$h = \epsilon_2 H$, $u_w = \epsilon_2^{3/2} \bar{U}_w$, $u_o = \epsilon_2^{3/2} \bar{U}_o$, $w_w = \epsilon_2^2 \bar{W}_w$, $w_o = \epsilon_2^2 \bar{W}_o$, and $t = \epsilon_2^{-1} \bar{T}$. At leading order in the new variables, the equations read

$$\bar{U}_{w_{ZZ}} = p_{w_{\bar{X}}} - \frac{1}{P^*} \Phi_{\bar{X}} \Phi_{ZZ}, \qquad \bar{U}_{w_{\bar{X}}} + \bar{W}_{w_Z} = 0, \qquad (93 \text{ a,b})$$

$$\mu^* \bar{U}_{o_{ZZ}} = p_{o_{\bar{X}}}, \qquad \bar{U}_{o_{\bar{X}}} + \bar{W}_{o_Z} = 0, \qquad (94 \text{ a,b})$$

$$p_{w_Z} = \frac{1}{P^*} \Phi_Z \Phi_{ZZ}, \qquad p_{o_Z} = 0, \qquad (95 \text{ a,b})$$

subject to

$$\bar{U}_w = \bar{W}_w = 0, \qquad\qquad\qquad Z = 0, \qquad (96)$$
$$\bar{U}_w = \bar{U}_o, \qquad \bar{W}_w = \bar{W}_o = \bar{U} H_{\bar{X}} + H_{\bar{T}}, \qquad \bar{U}_{w_Z} = \mu^* \bar{U}_{o_Z}, \qquad Z = H, \qquad (97)$$
$$p_w = p_o + \frac{1}{2P^*} \Phi_Z^2 - \frac{\Gamma}{2P^*} H_{\bar{X}\bar{X}}, \qquad Z = H, \qquad (98)$$
$$\bar{U}_{o_Z} \to 0, \qquad \bar{W}_{o_Z} \to 0, \qquad\qquad Z \to \infty. \qquad (99)$$

We also impose the constraint that $\mathbf{u}_w$ and p_w match with the velocity and pressure respectively as $X \to \pm\infty$. Note that (99) is the constraint that the velocity is bounded in the bulk of the oil.

Integrating (95b) in the oil phase yields $p_o = p_o(\bar{X}, \bar{T})$. By substituting this into (94a) and applying (99), we find that $\bar{U}_{o_Z} = 0$, and $p_{o_{\bar{X}}} = 0$. Hence, $\bar{U}_0 = \bar{U}_o(\bar{X}, \bar{T})$, and $p_o = p_o(\bar{T})$. By integrating (95a) and applying (98) we find that the pressure in the water layer is given by

$$p_w = p_o + \frac{1}{2P^*} \Phi_Z^2 |^- - \frac{\Gamma}{2P^*} H_{\bar{X}\bar{X}}. \qquad (100)$$

By substituting this into (93a), and applying (96) and (97), we find that the horizontal velocity in the thin water layer is given by

$$\bar{U}_w = \frac{1}{4P^*} (2Z - Z^2) \left(\Gamma H_{\bar{X}\bar{X}} + \frac{\sigma_{c0}^2 + 2s^* \sigma_{c0} \sigma_{o0} \cosh H + s^{*2} \sigma_{o0}^2}{\sinh^2 H} \right)_{\bar{X}}. \qquad (101)$$

By integrating (93b) from $Z = 0$ to $Z = H$, applying (96) and (97), and substituting in the expression (92), we obtain the following thin-film equation describing the thickness of the water layer, $H(Y)$, between the oil and the capillary wall,

$$H_{\bar{T}} + \left[\frac{H^3}{6P^*} \left(\Gamma H_{\bar{X}\bar{X}} + \frac{\sigma_{c0}^2 + 2s^* \sigma_{c0} \sigma_{o0} \cosh H + s^{*2} \sigma_{o0}^2}{\sinh^2 H} \right)_{\bar{X}} \right]_{\bar{X}} = 0. \qquad (102)$$

In the limit $\bar{X} \to -\infty$ we impose the condition that the solution approaches a constant value, H^*, to be determined. As $\bar{X} \to \infty$ we require the solution to match with the meniscus region. If we denote the radius of the meniscus by r^+ (non-dimensionalised with R), we assume that $r^+ \sim 1 - \epsilon_2 r_1^+ + \mathcal{O}(\epsilon_2^2)$. This is simply the condition that the radius of the meniscus is approximately the radius

18

of the capillary tube, and that the leading order correction, r_1^+, is of the order of the thickness of the wetting layer (the + superscripts denote the front meniscus). Hence, the boundary conditions we impose on H are $H \to H^*$ as $\bar{X} \to -\infty$, and $H_{\bar{X}\bar{X}} \to 1$ as $\bar{X} \to \infty$.

We assume a quasi-static travelling wave solution, $H(\bar{X}, \bar{T}) = H(Y)$, where $Y = \bar{X} - \bar{X}_R(\bar{T})$, and $\bar{X}_R$ is a reference point corresponding to the origin in the reference frame moving with the oil slug, which can be chosen arbitrarily. In the travelling wave coordinate, equation (102) becomes

$$P^* V H_Y = \left[\frac{H^3}{6} \left(\Gamma H_{YY} + \frac{\sigma_{c0}^2 + 2s^* \sigma_{c0} \sigma_{o0} \cosh H + s^{*2} \sigma_{o0}^2}{\sinh^2 H} \right)_Y \right]_Y, \qquad (103)$$

subject to

$$H \to H^* \qquad \qquad \text{as } Y \to -\infty, \qquad (104)$$
$$H_{YY} \to 1 \qquad \qquad \text{as } Y \to \infty, \qquad (105)$$

where $V = \mathrm{d}\bar{X}_R/\mathrm{d}\bar{T}$ is the velocity at which the oil slug moves. We integrate (103) once to arrive at the equation

$$6P^* V \frac{(H - H^*)}{H^3} = \Gamma H_{YYY} + \left(\frac{\sigma_{c0}^2 + 2s^* \sigma_{c0} \sigma_{o0} \cosh H + s^{*2} \sigma_{o0}^2}{\sinh^2 H} \right)_Y. \qquad (106)$$

Note that the unknown film thickness, H^*, appears in the boundary condition (104). However, it can be shown that (104) and (105) impose the required number of constraints to solve (106) for $H(Y)$, and to find H^*. (For details, see Appendix B.)

In the limit $Y \to -\infty$, we assume that $H \sim H^* + \bar{H}$, where $\bar{H}$ is a small perturbation. By substituting this into (106), applying $\bar{H} \to 0$ as $Y \to 0$, and using the translational invariance of the problem, we find that

$$H \sim H^* + e^{k_1 Y}, \qquad (107)$$

where k_1 is a root of the characteristic equation associated with the linear o.d.e. $\bar{H}$ satisfies. (For details, see Appendix B.) We will use this limiting behaviour of H as the initial condition when solving (106) via a shooting method in Section 4.1.

In the limit $Y \to \infty$, we assume that the radius of the meniscus is r^+, that is, we assume that $H_{YY} \sim \frac{1}{r^+}$. Thus the leading order term (in ϵ_2) is given by

$$H \sim \frac{1}{2}(Y + \alpha^+)^2 + r_1^+, \qquad (108)$$

for some constant α^+, which can be chosen arbitrarily due to the leading order translational invariance of the problem. From this we can compute the leading order correction to the radius of the meniscus, namely,

$$r_1^+ = \lim_{Y \to \infty} H - \frac{1}{2} H_Y^2. \qquad (109)$$

19

Hence, by solving (106) we are able to determine the thickness of the thin film region, H^*, the correction to the curvature in the front meniscus region, r_1^+, and the shape of the transition region, $H(Y)$, matching the two outer regions.

To find the shape of the oil-water interface at the rear end of the oil slug, we make the substitution $V \mapsto -V$ and solve (106) subject to (104) and (105). (This is equivalent to substituting $Y \mapsto -Y$.) In the limit $Y \to -\infty$, we assume that $H \sim H^* + \bar{H}$, where $\bar{H}$ is a small perturbation. By substituting this into (106), applying $\bar{H} \to 0$ as $Y \to 0$, and using the translational invariance of the problem, we find that

$$H \sim H^* + e^{k_1 Y} + A e^{k_2 Y}, \tag{110}$$

where k_1 and k_2 are roots of the characteristic equation associated the the linear o.d.e. satisfied by $\bar{H}$, and A is to be found.

In the limit $Y \to \infty$, we find that, similarly to the front of the oil slug, H satisfies

$$H \sim \frac{1}{2}(Y + \alpha^-)^2 + r_1^-. \tag{111}$$

Hence,

$$r_1^- = \lim_{Y \to \infty} H - \frac{1}{2}H_Y^2, \tag{112}$$

where α^- is an arbitrary constant corresponding to the translational invariance of the problem, and r_1^- is the leading order correction to the radius of curvature of the rear meniscus, $r^- \sim 1 - \epsilon_2 r_1^- + \mathcal{O}(\epsilon_2^2)$.

Note that as the film thickness, H^*, is determined by solving (106) at the front of the oil slug, it is not an unknown of the rear-end problem. However, (104) and (105) still impose the correct number of constraints, as the substitution $V \mapsto -V$ introduces the unknown variable A.

3.2.2 Solution when $P^* \ll 1$

In order to find an analytical expression for H^*, we consider the limit $P^* \ll 1$. Physically, this is the condition that the pressure difference across the capillary tube is less than the electrostatic pressure between the charged interfaces. In this limit, the shape of the oil slug will approximately be the shape at rest.

Integrating (106) yields

$$\Gamma H_{YY} + \frac{\sigma_{c0}^2 + 2s^* \sigma_{c0} \sigma_{o0} \cosh H + s^{*2} \sigma_{o0}^2}{\sinh^2 H} + 6 P^* V \int_Y^\infty \frac{H - H^*}{H^3} \mathrm{d}Y' = \Gamma. \tag{113}$$

By expanding $H \sim H_0 + P^* H_1 + \mathcal{O}(P^{*2})$, and $H^* \sim H_0^* + P^* H_1^* + \mathcal{O}(P^{*2})$, and considering the limit as $Y \to -\infty$ of (113), we find that, at leading order, the film thickness is given by

$$H_0^* = \cosh^{-1}\left(\frac{s^* \sigma_{c0} \sigma_{o0} + \sqrt{(\sigma_{c0}^2 + \Gamma)(s^{*2}\sigma_{o0}^2 + \Gamma)}}{\Gamma} \right). \tag{114}$$

Integrating (113), we find that

$$\frac{\Gamma}{2}H_Y^2 + \frac{2s^*\sigma_{c0}\sigma_{o0} + (\sigma_{c0}^2 + s^{*2}\sigma_{o0}^2)\cosh H^*}{\sinh H^*} - \frac{2s^*\sigma_{c0}\sigma_{o0} + (\sigma_{c0}^2 + s^{*2}\sigma_{o0}^2)\cosh H}{\sinh H}$$

$$+ 6P^*V \int_{-\infty}^{Y} H_Y \int_{Y'}^{\infty} \frac{H - H^*}{H^3} dY'' dY' = \Gamma(H - H^*).$$

(115)

By considering the leading order terms, in the limit $Y \to \infty$, we find that

$$H_0 \sim \frac{1}{2}\left(Y + \alpha^+\right)^2 + \left\{ H_0^* + \frac{\left(\sigma_{c0}^2 + s^{*2}\sigma_{o0}^2\right)}{\Gamma}\left(\coth H_0^* - 1\right) + \frac{2s^*\sigma_{c0}\sigma_{o0}}{\Gamma\sinh H_0^*} \right\}, \quad (116)$$

as $Y \to \infty$. Note that, by matching terms with (108), we see that the bracketed term in (116) gives the first order correction to the radius of the meniscus,

$$r_1^+ \sim H_0^* + \frac{\left(\sigma_{c0}^2 + s^{*2}\sigma_{o0}^2\right)}{\Gamma}\left(\coth H_0^* - 1\right) + \frac{2s^*\sigma_{c0}\sigma_{o0}}{\Gamma\sinh H_0^*} + \mathcal{O}(P^*). \quad (117)$$

As the oil slug is moving, the front and rear menisci have different radii, and hence, by the Laplace-Young equation (67), the pressure drop across the oil is dependent on the difference between these two radii. To find the correction to the meniscus radius at the rear end of the oil slug, we make the substitution $V \mapsto -V$. However, as the leading order correction to the radius of curvature (117) is independent of V, this correction term cancels out when considering the difference between the two ends the oil slug. Hence, the first order correction is required in order to find the leading order *difference* between the two ends.

By considering the $\mathcal{O}(P^*)$ terms in (115), in the limit $Y \to \infty$, we find that

$$H_1 \sim \frac{6V}{\Gamma} \int_{-\infty}^{\infty} \frac{(H_0 - H_0^*)^2}{H_0^3} dY', \quad (118)$$

as $Y \to \infty$. This is the $\mathcal{O}(P^*)$ correction to the radius of the meniscus. By making the substitution $V \mapsto -V$ for the rear-end calculations, the corrections to the menisci radii (up to $\mathcal{O}(P^*)$) are

$$r_1^{\pm} \sim H_0^* + \frac{\left(\sigma_{c0}^2 + s^{*2}\sigma_{o0}^2\right)}{\Gamma}\left(\coth H_0^* - 1\right) + \frac{2s^*\sigma_{c0}\sigma_{o0}}{\Gamma\sinh H_0^*} \pm \frac{6P^*V}{\Gamma}\int_{-\infty}^{\infty}\frac{(H_0 - H_0^*)^2}{H_0^3}dY',$$

(119)

where $\pm$ corresponds to the front and rear menisci, respectively.

We will now study the macroscopic problem to see how these corrections to the menisci radii, as well as the effect of having a thin water layer between the oil slug and the capillary wall, affect the oil slug's progression through the pore.

3.2.3   Macroscopic flux

In Sections 3.2.1 and 3.2.2, we focused on finding the shapes of the transition regions between the thin wetting film and the outer menisci, at the front and rear ends of the oil slug. In particular, we derived expressions for the thickness of the

wetting film, and for the corrections to the menisci radii in the limit $P^* \to 0$, (114) and (119) respectively. When solving for the flow of oil through the capillary on the macroscopic scale, the thin wetting film will be reduced to an effective boundary condition along the oil-clay interface, and the corrections to the menisci will affect the pressure jump across the oil-water interface at each end of the oil slug.

Returning to the macroscopic variables x, z, u_w, u_o, w_w, and w_o, the leading-order equations governing the fluid dynamics, (59) and (60), read

$$u_{wzz} = p_{wx}, \qquad p_{wz} = 0, \qquad u_{wx} + w_{wz} = 0, \qquad\qquad \text{(120 a,b,c)}$$

$$\mu^* u_{ozz} = p_{ox}, \qquad p_{oz} = 0, \qquad u_{ox} + w_{oz} = 0. \qquad\qquad \text{(121 a,b,c)}$$

There are five distinct regions in which we solve these equations, as shown in Figure 2. Region I is the bulk water region to the left hand side of the oil slug, $0 < x < x_r^*$, region II is the region primarily filled with oil, with a thin film of water coating the capillary walls, $x_c^* < x < x_c^* + L_o^*$, region III is the bulk water region to the right hand side of the oil slug, $x_f^* < x < 1$, region IV is the meniscus region at the rear of the oil slug, $x_r^* < x < x_c^*$, and region V is the meniscus region at the front of the oil slug, $x_c^* + L_o^* < x < x_f^*$. Note, however, that as the dimensional width of the meniscus regions is $\mathcal{O}(R)$, we find that $x_c^* - x_r^* = \mathcal{O}(\epsilon_1)$, and $x_f^* - x_c^* - L_o^* = \mathcal{O}(\epsilon_1)$, hence we can neglect regions IV and V from the macroscopic flux equations, and impose the Laplace-Young boundary condition, (67), on $x = x_c^*$ and $x = x_c^* + L_o^*$.

Letting P_1 and P_2 correspond to the pressures on the water side of the water-oil interfaces at $x = x_c^*$ and $x = x_c^* + L_o^*$, respectively, the boundary conditions (64)-(69) read

$$p_w = 1, \qquad\qquad\qquad \text{at } x = 0, \qquad \text{(122)}$$

$$p_w = P_1, \qquad p_o = P_1 + \frac{\Gamma}{2P^* r^-}, \qquad\qquad \text{at } x = x_c^*, \qquad \text{(123)}$$

$$p_w = P_2, \qquad p_o = P_2 + \frac{\Gamma}{2P^* r^+}, \qquad\qquad \text{at } x = x_c^* + L_o^*, \qquad \text{(124)}$$

$$p_w = 0, \qquad\qquad\qquad \text{at } x = 1, \qquad \text{(125)}$$

$$\mathbf{u}_w = 0, \qquad\qquad\qquad \text{at } z = 0, \qquad \text{(126)}$$

$$\mathbf{u}_w = \mathbf{u}_o, \qquad \mu^* u_{oz} = u_{wz}, \qquad p_w = p_o, \qquad \text{at } z = \epsilon_2 H^* \qquad \text{(127)}$$

$$p_z = u_{wz} = u_{oz} = w_w = w_o = 0, \qquad\qquad \text{at } z = 1. \qquad \text{(128)}$$

From (120b) and (121b), we see that $p_w = p_w(x)$ and $p_o = p_o(x)$. By integrating (120a) twice and applying (126) and (128), we find that in regions I and III,

$$u_w = p_{wx} \left(\frac{1}{2} z^2 - z \right). \qquad\qquad \text{(129)}$$

Integrating (120a) and (121a), subject to (126)-(128), yields, correct to $\mathcal{O}(\epsilon_2)$,

$$u_w = p_x \left(\frac{1}{2} z^2 + (\epsilon_2 H^* (\mu^* - 1) - \mu^*) z \right) \qquad\qquad 0 < z < \epsilon_2 H^*, \qquad \text{(130)}$$

$$u_o = \frac{1}{\mu^*} p_x \left(\frac{1}{2} z^2 - z + \epsilon_2 H^* (1 - \mu^*) \right) \qquad\qquad \epsilon_2 H^* < z < 1, \qquad \text{(131)}$$

22

in region II. By integrating (120c) from $z = 0$ to $z = 1$ in regions I and III, (120c) from $z = 0$ to $z = \epsilon_2 H^*$ in region II, (121c) from $z = \epsilon_2 H^*$ to $z = 1$ in region II, and applying (126)-(128), we find that

$$\frac{\partial}{\partial x}\left[\int_0^1 u_w \mathrm{d}z\right] = 0, \qquad \text{in regions I, III,} \qquad (132)$$

$$\frac{\partial}{\partial x}\left[\int_0^{\epsilon_2 H^*} u_w \mathrm{d}z + \int_{\epsilon_2 H^*}^1 u_o \mathrm{d}z\right] = 0, \qquad \text{in region II.} \qquad (133)$$

Hence it follows that that $p_{xx} = 0$ for $0 < x < 1$, i.e. the pressure gradient is constant. Using u_w and u_o, given by (129) - (131), and integrating (132) and (133), we find that, correct to $\mathcal{O}(\epsilon_2)$,

$$Q_w = -\frac{1}{3}p_x, \qquad \text{in regions I, III,} \qquad (134)$$

$$Q_w = 0, \qquad \text{in region II} \qquad (135)$$

$$Q_o = -\frac{1}{\mu^*}p_x\left(\frac{1}{3} - \epsilon_2(1 - \mu^*)H^*\right), \qquad \text{in region II,} \qquad (136)$$

where $Q_w = \int u_w \mathrm{d}z$ and $Q_o = \int u_o \mathrm{d}z$ are the volumetric flow rates of water and oil, respectively, in the lower half of the capillary tube. Hence, by applying (122) - (125) to $p_{xx} = 0$, we find that correct to $\mathcal{O}(\epsilon_2)$ in regions I, II, and III,

$$Q_w = \frac{1}{3x_c^*}(1 - P_1), \qquad\qquad\qquad \text{I} \qquad (137)$$

$$Q_o = \frac{1}{\mu^* L_o^*}\left\{\frac{P_1 - P_2}{3} + \epsilon_2\left[\frac{\Gamma}{6P^*}(r_1^- - r_1^+) - (P_1 - P_2)(1 - \mu^*)H^*\right]\right\}, \qquad \text{II} \qquad (138)$$

$$Q_w = \frac{1}{3(1 - x_c^* - L_o^*)}P_2, \qquad\qquad\qquad \text{III} \qquad (139)$$

respectively. (In region II, $Q_w = \mathcal{O}(\epsilon_2^2)$, so we neglect this term.)

Since we assume that the slug fills almost the whole width of the channel, we have that by conservation of volume $Q := Q_o \sim Q_w$. Hence, by solving the three equations, (137) - (139), for the three unknowns, P_1, P_2, and Q, we find that

$$Q \sim \frac{1}{1 + (\mu^* - 1)L_o^*}\left\{\frac{1}{3} + \epsilon_2\left[\frac{\Gamma}{6P^*}(r_1^- - r_1^+) + \frac{\mu^* L_o^*}{1 + (\mu^* - 1)L_o^*}(\mu^* - 1)H^*\right]\right\}. \qquad (140)$$

To derive expressions for $r_1^\pm$ and H^*, we solve (106) subject to (104) and (105). However, as V is the speed at which the slug is moving, $Q = Q_o = V$. Hence, (106) is dependent on Q. In order to solve (106) and (140), we expand $Q \sim Q_0 + \epsilon_2 Q_1 + \mathcal{O}(\epsilon_2^2)$, and $V \sim V_0 + \epsilon_2 V_1 + \mathcal{O}(\epsilon_2^2)$. At leading order in ϵ_2, we find that (140) reduces to

$$Q_0 = V_0 = \frac{1}{3}\left[\frac{1}{1 + (\mu^* - 1)L_o^*}\right]. \qquad (141)$$

Substituting this expression for V_0 into (106), and solving subject to (104) and (105), yields the profile of the front meniscus region, $H(Y)$, at leading order in ϵ_2. In particular, this gives us H^*, and, by using (109), $H(Y)$ can be used to find r_1^+. To find r_1^-, we solve (106) subject to (104) and (105) with the substiution $V_0 \mapsto -V_0$, and the obtained value of H^* in (104). From this we obtain $H(Y)$, and consequently we compute r_1^- using (112).

The first-order correction to the volumetric flow rate, $Q_1 = V_1$, is then found from (140), namely

$$Q_1 = V_1 = \frac{1}{1 + (\mu^* - 1)L_o^*} \left\{ \frac{\Gamma}{6P^*}(r_1^- - r_1^+) + \frac{\mu^* L_o^*}{1 + (\mu^* - 1)L_o^*}(\mu^* - 1)H^* \right\}. \quad (142)$$

For $P^* \ll 1$, we can make use of the expressions (114) and (119) to get that

$$Q = V \sim \frac{1}{1 + (\mu^* - 1)L_o^*} \left\{ \frac{1}{3} + \right.$$
$$\left. \epsilon_2 \frac{1}{1 + (\mu^* - 1)L_o^*} \left[L_o^* \mu^* (\mu^* - 1)H_0^* - \frac{2}{3} \int_{-\infty}^{\infty} \frac{(H_0 - H_0^*)^2}{H_0^3} \mathrm{d}Y' \right] \right\}. \quad (143)$$

It should be noted that due to the integral term, even in this asymptotic limit, (106) needs to be solved numerically. However, this computation is made significantly simpler for two reasons. First, as the integral term occurs in the first-order (in P^*) correction to the meniscus radius, we only require the leading order term of the integral (as we have neglected $\mathcal{O}(P^{*2})$ terms). Hence, we set the left-hand side of (106) to zero, integrate twice to obtain (115) (with P^* set to zero), and thus we only need to solve a first-order ode for H. Second, since we have an expression for the film thickness, (114), we can solve (115) as an initial value problem, whereas for the full numerical solution we need to use a shooting method, as this boundary condition is unknown.

4 Numerical Solution

In Section 4.1, we describe how to solve (106) subject to (104) and (105) numerically to find the shape of the front and rear ends of the oil slug, for $P^* = \mathcal{O}(1)$. In Section 4.2, we describe how to find the volumetric flow rate of the oil slug, Q, using the solution obtained in Section 4.1. We plot Q and the film thickness, h^*, for different values of P^* as the salinity is varied.

To study the effect of having different materials on the two surfaces, we introduce a dimensionless parameter, χ, such that $K_{of}^{1,2}/K_{or}^{1,2} = \chi K_{of}^{1,2}/K_{or}^{1,2}$. This parameter is a measure of the reactiveness of the oil-water interface with the ions, relative to the clay-water interface. Unless stated otherwise, we will set $\chi = 10^{-3}$.

We will plot Q and h^* against P^*, to compare the numerical solution for $P = \mathcal{O}(1)$ with the asymptotic solution in the limit $P^* \to 0$. In the computations we choose $L_o^* = 0.5$ and $s_o^* = s_c^*$, and, except where stated otherwise, use the parameter values given in Appendix A.

As the dimensionless parameters, $\mathcal{K}_c^{1,2} = K_{cf}^{1,2} c_\infty^{1,2+}/K_{cr}^{1,2}$, $\mathcal{K}_o^{1,2} = K_{of}^{1,2} c_\infty^{1,2+}/K_{or}^{1,2}$, and $\epsilon_2 = (\varepsilon_w k_B T/2(c_\infty^1 + 4c_\infty^2)q^2)^{1/2}/R$ depend on the concentration of ions, $c_\infty^{1,2}$,

in order to vary the salinity in our numerical computations, we must vary these parameters simultaneously. We define $c_{low}^{1,2}$ to be the bulk concentrations of monovalent and divalent ions, respectively, in the low salinity regime, and $c_{high}^{1,2}$ to be the bulk concentrations of monovalent and divalent ions, respectively, in the high salinity regime.

We define intermediate concentrations by $c_{int}^{1,2} = c_{low}^{1,2} + 10^\tau (c_{high}^{1,2} - c_{low}^{1,2})$, for a parameter $\tau \in (-\infty, 0]$. (We choose a power law for τ as the concentrations span multiple orders of magnitude.) By defining the dimensionless parameters in the problem using $c_{int}^{1,2}$ instead of $c_\infty^{1,2}$, we get that the dimensionless parameters in the intermediate regimes are related to the dimensionless parameters in the low salinity regime by

$$\mathcal{K}_c^{1,2}{}_{int} = \mathcal{K}_c^{1,2}{}_{low} \left(1 + 10^\tau \left(\frac{c_{high}^{1,2}}{c_{low}^{1,2}} - 1 \right) \right), \tag{144}$$

$$\mathcal{K}_o^{1,2}{}_{int} = \mathcal{K}_o^{1,2}{}_{low} \left(1 + 10^\tau \left(\frac{c_{high}^{1,2}}{c_{low}^{1,2}} - 1 \right) \right), \tag{145}$$

$$\epsilon_{2int} = \epsilon_{2low} \left(1 + 10^\tau \left(\frac{c_{high}^1 + 4c_{high}^2}{c_{low}^1 + 4c_{low}^2} - 1 \right) \right)^{-1/2}. \tag{146}$$

Hence, using τ, we can study the effect of varying the salinity with a single parameter. In the limit $\tau \to -\infty$ we recover the low salinity regime, and for $\tau = 0$ we recover the high salinity regime. In the computations we approximate $\tau = -\infty$ by $\tau = -6$.

4.1 Shape of the oil-water interface

To find the shape of the oil-water interface at the front end of the oil slug, we solve (106) subject to (104), (105), and (141) using a shooting method, since the thickness of the wetting layer, H^*, is unknown a priori. We use the form of H as $Y \to -\infty$, (107), and its derivatives as the initial values in (106), with an initial guess for H^*. We use an RK4 method to solve (106) for $H(Y)$, compute the limit of the curvature, H_{YY}, as $Y \to \infty$, and vary H^* until this is equal to 1.

To find the shape of the oil-water interface at the rear end of the oil slug, we solve (106) subject to (104), (105), and (141), with the substitution $V \mapsto -V$. Again, we use a shooting method with the form of H as $Y \to -\infty$, (110), and its derivatives as the initial values. However, for the rear-end computation, we use A as the shooting parameter, as H^* is determined by the solution at the front end of the oil slug. We use an RK4 method to solve (106) for $H(Y)$, compute the limit of the curvature, H_{YY}, as $Y \to \infty$, and vary A until this is equal to 1.

In Figure 4, we plot the front and rear transition rear profiles, $H(Y)$, for $P = 1.4 \cdot 10^{-4}, 1, 10, 20$. We see that the front meniscus is always monotonic, but that non-monotonic solutions are possible for the rear meniscus. This is because the characteristic equation of (106) under a perturbation, $H = H^* + \bar{H}$, admits imaginary solutions for $V < 0$.
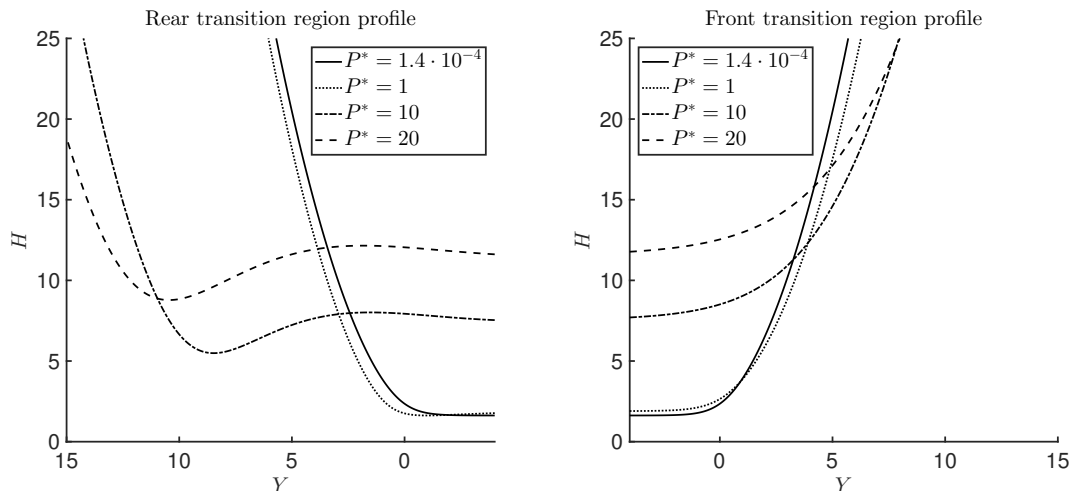
Figure 4: Plots of the rear and front oil-water interface profiles, $H(Y)$, in the low salinity regime, $\tau = -6$, for $P = 1.4 \cdot 10^{-4}, 1, 10, 20$.

4.2 Velocity of the oil slug

To find the velocity of the oil slug correct to $\mathcal{O}(\epsilon_2)$, we use the method described in Section 4.1 to determine the profile of the front and rear menisci, $H^{\pm}(Y)$ respectively, and the film thickness, H^*. By substituting $H^+(Y)$ into (109), and $H^-(Y)$ into (112), we obtain the first order corrections to the front and rear radii of curvature, $r_1^{\pm}$. Hence, we determine the velocity of the oil slug by substituting H^* and $r^{\pm}$ into (140).

In Figure 5(a), we plot the volumetric flow rate, Q, against the bulk concentration of ions, varying the salinity from low salinity, $\tau = -6$, to high salinity, $\tau = 0$. We see that the flow rate increases by approximately 7% when the salinity is reduced, suggesting that this mechanism may contribute to the low salinity effect.

In Figure 5(b), we plot the film thickness, $h^* = \epsilon_2 H^*$, as a function of the salinity, for the same range of salinities as in Figure 5(a). We choose the rescaling, $h^* = \epsilon_2 H^*$, so that the choice of non-dimensionalisation does not depend on the Debye length (and hence the salinity). We see that h^* increases from $1.2 \cdot 10^{-5}$ to $2.5 \cdot 10^{-3}$ as the salinity decreases, which corresponds to a dimensional thickness ranging from $1.2 \cdot 10^{-11}$ m to $2.5 \cdot 10^{-9}$ m. The low salinity estimates are of a similar order of magnitude to experimental results (for example, see Lee et al. [16], who found that the thickness ranges from $8 \cdot 10^{-10}$ m to $1.5 \cdot 10^{-9}$ m). However, the high salinity estimate is significantly lower, by approximately two orders of magnitude. One possible explanation for this discrepancy is that at high salinities the film thickness becomes comparable with the size of the ions, and the continuum assumption no longer applies. The finite ion size creates an additional repulsion between the surfaces, which will lead to the continuum approximation underestimating the thickness of the water film. It is also likely that there is considerable error in estimates for the saturation concentrations and the dissociation constants, s_c^*, s_o^*, $K_{fc}^{1,2}$, $K_{rc}^{1,2}$, $K_{fo}^{1,2}$, and $K_{ro}^{1,2}$.
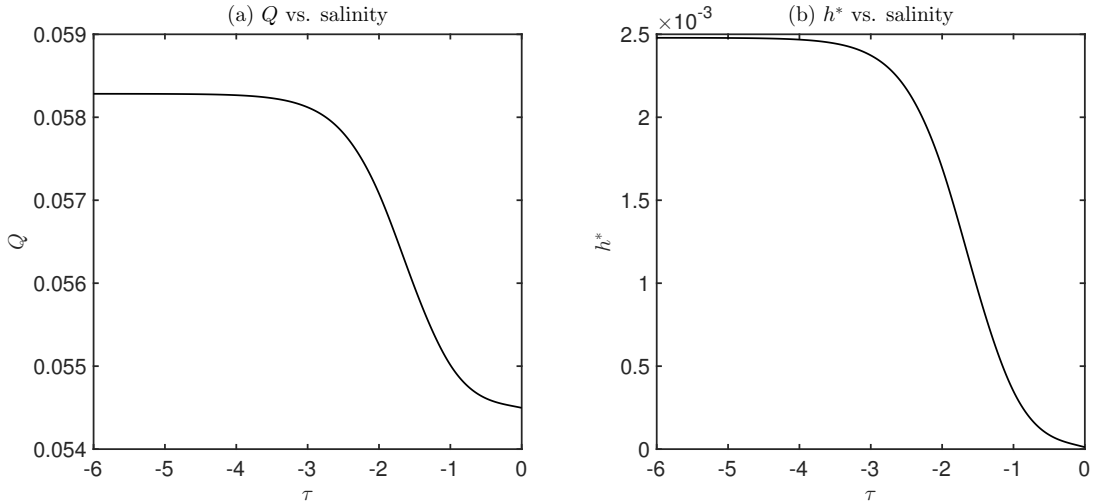
Figure 5: Plots of the volumetric flow rate, Q, and the film thickness, h^*, as the salinity is varied, found by solving (106) and (140) numerically, subject to (104) and (105).

We study the effect of varying s_c^* by varying Γ (as $\Gamma = 2\gamma\varepsilon_w R/L^2 q^2 s_c^{*2}$). In Figure 6, we plot the film thickness, h^*, against Γ, for $\tau = -1.3$, and $c^* = 0, 0.1$ (as this corresponds to a 0.1M solution of NaCl with and without trace amounts of divalent ions, at concentrations of 0M, and 0.01M respectively, which we can use to compare with the results of Lee et al. [16]). We see that in the presence of divalent ions at a concentration of 0.01M, the film thickness is bounded by approximately $6.7 \cdot 10^{-4}$. However, when divalent ions are not present, the film thickness appears to be unbounded. As the film thickness is sensitive to trace amounts of divalent ions, in order to compare the theory with the results of Lee et al., a more detailed breakdown of the composition of the brine used is required. However, the increase in the film thickness observed with the removal of the divalent ions is consistent with the MIE mechanism.

In Figure 7(a), we compare the numerical solution for Q, given by (106) and (140), subject to (104) and (105), with the asymptotic solution in the limit $P^* \to 0$, given by (143), for P^* ranging from 10^{-5} to 1. We see that the numeric solution agrees with the asymptotic solution to within 0.2% for $P^* < 1$. In Figure 7(b), we compare the asymptotic expression for the film thickness, H^*, in the limit $P^* \to 0$, (114), with the numerically computed values. There is agreement to within 2%, for $P^* < 0.1$.

5   Conclusion and Discussion

In this paper, we have presented a model for the steady motion of an oil slug through a pore throat, assuming that low salinity oil recovery can be explained by multicomponent ionic exchange (MIE). Transient effects were neglected by assuming Re $\ll$ 1. We also assumed that the rates at which the ions react with the surfaces are fast in comparison to the typical relaxation time of the charged
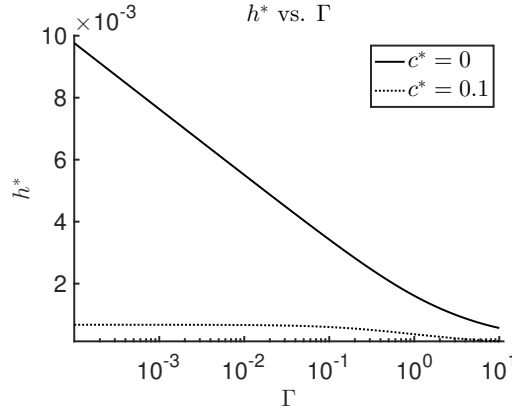
Figure 6: Plots of the film thickness, h^*, as Γ, is varied, for $\tau = -1.3$ and $c^* = 0, 0.1$, found by solving (106) and (140) numerically, subject to (104) and (105). The solid line, $c^* = 0$, represents a pure 0.1M solution of NaCl, and the dotted line, $c^* = 0.1$, represents a 0.1M solution of NaCl containing 0.01M CaCl$_2$.

surfaces in the viscous fluid.

We obtained an analytic expression for the velocity of the oil slug, (140), assuming that the aspect ratio of the oil slug was small. Further, in the asymptotic limit $P^* \ll 1$ ($P^* = \varepsilon_w P / q^2 s_c^{*2}$), a simplified expression (143) for the velocity was derived, as well as an analytical expression for the thickness of the wetting film between the oil and the capillary, (114).

$$H_0^* = \cosh^{-1}\left(\frac{s^* \sigma_{c0}\sigma_{o0} + \sqrt{(\sigma_{c0}^2 + \Gamma)(s^{*2}\sigma_{o0}^2 + \Gamma)}}{\Gamma}\right), \tag{114}$$

$$Q_0 = V_0 = \frac{1}{3}\left[\frac{1}{1 + (\mu^* - 1)L_o^*}\right], \tag{140}$$

$$Q = V \sim \frac{1}{1 + (\mu^* - 1)L_o^*}\left\{\frac{1}{3} + \right.$$
$$\left. \epsilon_2 \frac{1}{1 + (\mu^* - 1)L_o^*}\left[L_o^*\mu^*(\mu^* - 1)H_0^* - \frac{2}{3}\int_{-\infty}^{\infty}\frac{(H_0 - H_0^*)^2}{H_0^3}dY'\right]\right\}. \tag{143}$$

Numerical results showed that for the values considered, the flow rate increases by approximately 7% when transitioning from high salinity to low salinity regimes, which could contribute to the increase in oil recovery often observed in core scale experiments.

While care was taken to estimate reasonable values for the parameters, one of the main limitations of our numerical results is that the values of s_o^*, s_c^*, $\mathcal{K}_c^k$, and $\mathcal{K}_o^k$, for $k = 1, 2$, are difficult to estimate without more data, and can have a significant impact on the theoretical results obtained. An experimental investigation to determine the correct values of these parameters would improve the accuracy of the results.
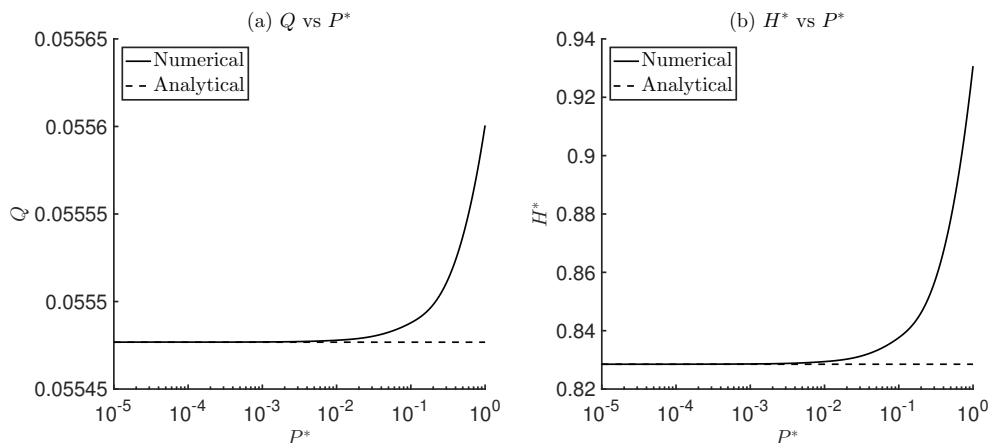
28

Figure 7: Plots of the volumetric flow rate, Q, and the film thickness, H^*, against P^*, for $10^{-5} < P^* < 1$, in the 0.1M NaCl regime, $\tau = -1.3$. The solid lines represent the numerical solutions to (106) and (140), subject to (104) and (105), and the dashed lines represent the asymptotic solutions, (143) and (114), in the limit $P^* \to 0$.

Another issue is due to the fact that, as the salinity decreases, the Debye length, λ, increases. If λ becomes too large, then we can no longer make the assumption that $\epsilon_2 = \lambda/R$ is small, and hence (140) is no longer valid. The system (59)-(69) then needs to be solved numerically. On the other hand, as λ decreases, the width of the water film becomes comparable to the size of the ions. This will restrict the movement of ions in and out of the water film, reducing the effect of the low salinity injection. At some point, the continuum model will break down, and an alternative model for ion movement in the thin film would need to be considered.

In order to get an accurate estimate of how the increase in velocity due to low salinity effects at the pore scale would affect flow in an oil reservoir, a larger scale model needs to be developed. Our future aim is to homogenise the pore scale model described in this paper, assuming a microscopic network of capillaries containing flow governed by (140), to describe the flow at the core scale in order to address the flow over larger length scales. Further, due to the similarities between the MIE and pH increase mechanisms, by considering different reactions in place of (20) and (21), and following the same procedure, different mechanisms for the low salinity oil recovery process can be compared. The benefit of such models is the ability to translate chemical-scale mechanisms into core-scale results. By comparing experimental results with such a model, we hope to obtain a better understanding of the low salinity process.

Acknowledgements

Appendix A

Dimensional Parameters			
Parameter	Value	Reference	Notes
c_∞^1	$1 \cdot 10^{25} - 1 \cdot 10^{27}$ m^{-3}	[1]	
c_∞^2	$3 \cdot 10^{24} - 5.4 \cdot 10^{25}$ m^{-3}	[1]	
R	10^{-6} m	[23]	
L	10^{-5} m	[23]	
λ	$1.5 \cdot 10^{-9} - 2 \cdot 10^{-10}$ m		$\lambda = \left(\varepsilon_w k_B T / 2\left(c_\infty^1 + 4c_\infty^2\right)q^2\right)^{-1/2}$
γ	0.02 J m^{-2}	[5]	
μ_o	0.01 kg m^{-1} s^{-1}	[5]	
μ_w	$8.9 \cdot 10^{-4}$ kg m^{-1} s^{-1}	[5]	
ρ_o	850 kg m^{-3}	[5]	
ρ_w	1000 kg m^{-3}	[5]	
P	0.7 N m^{-2}		$P \sim 8\mu_w L V / R^2$
T	$375°$K	[15]	
$D^{\pm,2\pm}$	$7.9 \cdot 10^{-10} - 2 \cdot 10^{-9}$ m^2 s^{-1}	[28]	
s_c^*	10^{16} m^{-2}	[17]	Estimate using $\sigma_c = q s_c^*$.
s_o^*	10^{16} m^{-2}	[17]	Estimate using $\sigma_o = q s_o^*$.
$K_{c_f}^1 / K_{c_r}^1$	$3 \cdot 10^{-28}$ m^3	[17]	See Section 3.1.2.
$K_{c_f}^2 / K_{c_r}^2$	$4.1 \cdot 10^{-25}$ m^3	[17]	See Section 3.1.2.
$K_{o_f}^1 / K_{o_r}^1$	$3 \cdot 10^{-31}$ m^3	[17]	See Section 3.1.2.
$K_{o_f}^2 / K_{o_r}^2$	$4.1 \cdot 10^{-28}$ m^3	[17]	See Section 3.1.2.
ε_{wr}	56	[19]	
ε_0	$8.9 \cdot 10^{-12}$ C^{2}J^{-1} m^{-1}		
q	$1.6 \cdot 10^{-19}$ C		
k_B	$1.4 \cdot 10^{-23}$ J K^{-1}		

| Dimensionless Parameters			
Parameter	Value	Expression	Notes
ϵ_1	0.1	R/L	
ϵ_2	$1.5 \cdot 10^{-3} - 2 \cdot 10^{-4}$	λ/R	
Re	$8.8 \cdot 10^{-4}$	$\rho_w P R^2 / \mu_w^2$	
Pe$^{\pm,2\pm}$	$0.39 - 1$	$PR^2 / D^{\pm,2\pm}\mu_w$	
δ	$10^{-3} - 10^{-5}$	$s_c^* / c_\infty^1 R$	
P^*	$1.4 \cdot 10^{-4}$	$\varepsilon_w P / q^2 s_c^{*2}$	
ξ	98	$q^2 s_c^* R / \varepsilon_w k_B T$	
ρ^*	0.85	ρ_o / ρ_w	
μ^*	11	μ_o / μ_w	
c^*	$0.3 - 0.05$	c_∞^2 / c_∞^1	
$\Lambda_c^{1,2}$	$\ll 1$	$PR^2 / \mu_w L^2 K_{c_r}^{1,2}$	Assume reactions are fast.
$\Lambda_o^{1,2}$	$\ll 1$	$PR^2 / \mu_w L^2 K_{o_r}^{1,2}$	Assume reactions are fast.
$\mathcal{K}_c^1$	$3.3 \cdot 10^{-3} - 3.3 \cdot 10^{-1}$	$K_{c_f}^1 c_\infty^1 / K_{c_r}^1$	
$\mathcal{K}_c^2$	$1.2 - 22$	$K_{c_f}^2 c_\infty^2 / K_{c_r}^2$	
$\mathcal{K}_o^1$	$3.3 \cdot 10^{-6} - 3.3 \cdot 10^{-3}$	$K_{o_f}^1 c_\infty^1 / K_{o_r}^1$	
$\mathcal{K}_o^2$	$1.2 \cdot 10^{-3} - 2.2 \cdot 10^{-2}$	$K_{o_f}^2 c_\infty^2 / K_{o_r}^2$	
Γ	0.08	$2\gamma \varepsilon_w R / L^2 q^2 s_c^{*2}$	
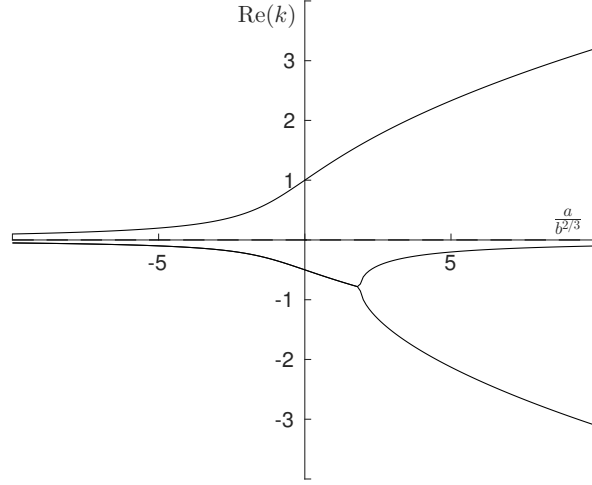
Figure 8: Plot of the real parts of the roots of (151) as $\frac{a}{b^{2/3}}$ varies.

Appendix B

At first glance it may appear that there are not enough boundary conditions to solve the third order differential equation, (106). In order to examine this, we consider the behaviour of H as $Y \to \pm\infty$.

As $Y \to -\infty$, we suppose that $H = H^* + \bar{H}$, for some small $\bar{H}(Y)$, and we find that the perturbation satisfies

$$\bar{H}_{YYY} - a\bar{H}_Y - b\bar{H} = 0, \tag{147}$$

where

$$a = \frac{2}{\Gamma \sinh^3 H^*} \left[(s^{*2}\sigma_{o0}^2 + \sigma_{c0}^2) \cosh H^* + (\cosh^2 H^* + 1)s^*\sigma_{o0}\sigma_{c0} \right], \tag{148}$$

$$b = \frac{6P^*V}{\Gamma H^{*3}}. \tag{149}$$

The solution to this is given by

$$\bar{H} = A_1 e^{k_1 Y} + A_2 e^{k_2 Y} + A_3 e^{k_3 Y}, \tag{150}$$

where k_i are the roots of $k^3 - ak - b = 0$. By rescaling $k = b^{1/3}\hat{k}$, we can show that finding these roots is equivalent to finding the roots of

$$\hat{k}^3 - \frac{a}{b^{2/3}}\hat{k} - 1 = 0. \tag{151}$$

This equation has precisely two roots with negative real part, and one root with positive real part, for any real value of $ab^{-2/3}$. A plot of the real part of these roots is given in Figure 8.

31

We require $\bar{H}$ to decay as $Y \to -\infty$. At the front meniscus, $V > 0$, so $b > 0$; hence, the coefficients of the two exponentials corresponding to the roots with negative real part must be zero. For this reason, the boundary condition $H \to H^*$ (for unknown H^*) as $Y \to -\infty$ eliminates two degrees of freedom of the solution, rather than one.

By translational invariance, we can set the final coefficient in (150) to be unity without loss of generality. Hence, as $Y \to -\infty$ in the front meniscus region, the film thickness is given by

$$H \sim H^* + e^{k_1 Y}. \tag{152}$$

The remaining degree of freedom, H^*, is constrained by the condition $H_{YY} \to 1$ as $Y \to \infty$. Hence, the two boundary conditions (104) and (105) are sufficient to solve (106) (for $V > 0$, i.e. at the front of the oil slug), and to determine H^*. Numerically, we find H^* by using a shooting method. That is, we treat (106) as an initial value problem, using (152) as the initial value, and vary H^* until $\lim_{Y \to \infty} H_{YY} = 1$.

At the rear meniscus, we solve the same differential equation with $V < 0$. Hence, $b < 0$, so $k = b^{1/3}\hat{k}$ has only one root with negative real part, and thus only one coefficient is determined (to be zero) in (150). After setting one of the remaining coefficients to be unity by translational invariance, there is still one coefficient that needs to be determined. Explicitly,

$$H \sim H^* + e^{k_1 Y} + A e^{k_2 Y}, \tag{153}$$

as $Y \to -\infty$, for some A to be determined. Since H^* is determined by the solution to the equation at the front meniscus, this leaves one unknown to be found. This additional constraint comes from the condition $H_{YY} \to 1$ as $Y \to \infty$. Hence, (104) and (105) are sufficient to solve (106) for $V < 0$, provided H^* is known. This is what we expect; the shape of the front end of the oil slug determines the film thickness, which in turn determines the shape of the rear end of the oil slug, i.e. the information travels in the direction of the flow.

To determine A numerically, we solve (106) using a shooting method, similarly to the $V > 0$ case. We use (153) as the initial value, and vary A until $\lim_{Y \to \infty} H_{YY} = 1$.

References

[1] T. Austad, A. RezaeiDoust, T. Puntervold, et al. Chemical mechanism of low salinity water flooding in sandstone reservoirs. In *SPE improved oil recovery symposium*. Society of Petroleum Engineers, 2010.

[2] D. Ben-Yaakov and D. Andelman. Revisiting the poisson–boltzmann theory: Charge surfaces, multivalent ions and inter-plate forces. *Physica A: Statistical Mechanics and its Applications*, 389(15):2956–2961, 2010.

[3] S. Berg, A. Cense, E. Jansen, K. Bakker, et al. Direct experimental evidence of wettability modification by low salinity. *Petrophysics*, 51(05), 2010.

[4] F. Bretherton. The motion of long bubbles in tubes. *J. Fluid Mech*, 10(2):166–188, 1961.

[5] J. S. Buckley. *Mechanisms and consequences of wettability alteration by crude oils.* PhD thesis, Heriot-Watt University, 1996.

[6] B. Derjaguin and L. Landau. Theory of the stability of strongly charged lyophobic sols and of the adhesion of strongly charged particles in solutions of electrolytes. *Progress in Surface Science*, 43(1):30–59, 1993.

[7] A. G. Egorov, K. G. Kornev, and A. V. Neimark. Meniscus motion in a prewetted capillary. *Physics of Fluids (1994-present)*, 15(10):3134–3143, 2003.

[8] G. Hirasaki et al. Wettability: fundamentals and surface forces. *SPE Formation Evaluation*, 6(02):217–226, 1991.

[9] P. Jadhunandan. *Effects of brine composition, crude oil, and aging conditions on wettability and oil recovery.* Department of Petroleum Engineering, New Mexico Institute of Mining & Technology, 1990.

[10] P. Jadhunandan and N. Morrow. Spontaneous imbibition of water by crude oil/brine/rock systems. *In Situ;(United States)*, 15(4), 1991.

[11] P. Jadhunandan, N. Morrow, et al. Effect of wettability on waterflood recovery for crude-oil/brine/rock systems. *SPE reservoir engineering*, 10(01):40–46, 1995.

[12] A. Kovscek, H. Wong, and C. Radke. A pore-level scenario for the development of mixed wettability in oil reservoirs. *AIChE Journal*, 39(6):1072–1085, 1993.

[13] I. Kuchin, O. Matar, R. Craster, and V. Starov. Influence of the disjoining pressure on the equilibrium interfacial profile in transition zone between a thin film and a capillary meniscus. *Colloids and Interface Science Communications*, 1:18–22, 2014.

[14] I. V. Kuchin, O. K. Matar, R. V. Craster, and V. M. Starov. Modeling the effect of surface forces on the equilibrium liquid profile of a capillary meniscus. *Soft matter*, 10(32):6024–6037, 2014.

[15] A. Lager, K. Webb, C. Black, M. Singleton, and K. Sorbie. Low salinity oil recovery–an experimental investigation. *Petrophysics*, 49(1):28, 2008.

[16] S. Lee, K. Webb, I. Collins, A. Lager, S. Clarke, M. O'Sullivan, A. Routh, X. Wang, et al. Low salinity oil recovery: Increasing understanding of the underlying mechanisms. 2010.

[17] S. Li and R. Xu. Electrical double layers interaction between oppositely charged particles as related to surface charge density and ionic strength. *Colloids and Surfaces A: Physicochemical and Engineering Aspects*, 326(3):157–161, 2008.

[18] D. J. Ligthelm, J. Gronsveld, J. Hofman, N. Brussee, F. Marcelis, H. van der Linde, et al. Novel waterflooding strategy by manipulation of injection brine composition. In *EUROPEC/EAGE Conference and Exhibition*. Society of Petroleum Engineers, 2009.

[19] C. Malmberg and A. Maryott. Dielectric constant of water from 00 to 1000 c. *J Res Nat Bureau Stand*, 56:1–8, 1956.

[20] D. McCormack, S. Carnie, and D. Chan. Calculations of electric double-layer force and interaction free energy between dissimilar surfaces. *Journal of Colloid and Interface Science*, 169(1):177–196, 1995.

[21] P. McGuire, J. Chatham, F. Paskvan, D. Sommer, F. Carini, et al. Low salinity oil recovery: An exciting new eor opportunity for alaska's north slope. In *SPE Western Regional Meeting*. Society of Petroleum Engineers, 2005.

[22] N. R. Morrow et al. Wettability and its effect on oil recovery. *Journal of Petroleum Technology*, 42(12):1–476, 1990.

[23] P. Nelson. Pore-throat sizes in sandstones, tight sandstones, and shales. *AAPG bulletin*, 93(3):329–340, 2009.

[24] H. Ohshima. Diffuse double layer interaction between two parallel plates with constant surface charge density in an electrolyte solution i. *Colloid and Polymer Science*, 252(3):158–164, 1974.

[25] H. Ohshima. Diffuse double layer interaction between two parallel plates with constant surface charge density in an electrolyte solution ii. *Colloid and Polymer Science*, 252(3):257–267, 1974.

[26] V. Parsegian and D. Gingell. On the electrostatic interaction across a salt solution between two bodies bearing unequal charges. *Biophysical journal*, 12(9):1192, 1972.

[27] A. RezaeiDoust, T. Puntervold, and T. Austad. Chemical verification of the eor mechanism by using low saline/smart water in sandstone. *Energy & Fuels*, 25(5):2151–2162, 2011.

[28] E. Samson, J. Marchand, and K. Snyder. Calculation of ionic diffusion coefficients on the basis of migration test results. *Materials and Structures*, 36(3):156–165, 2003.

[29] L. Tanner. The spreading of silicone oil drops on horizontal surfaces. *Journal of Physics D: Applied Physics*, 12(9):1473, 1979.

[30] E. Verwey and J. Overbeek. *Theory of the stability of lyophobic colloids.* Courier Corporation, 1999.

[31] H. Wong, S. Morris, and C. Radke. Three-dimensional menisci in polygonal capillaries. *Journal of Colloid and Interface Science*, 148(2):317–336, 1992.

[32] H. Yildiz. *Effect of brine composition on oil recovery by waterflooding.* Department of Petroleum Engineering, New Mexico Institute of Mining & Technology, 1995.

[33] H. Yildiz and N. Morrow. Effect of brine composition on recovery of moutray crude oil by waterflooding. *Journal of Petroleum science and Engineering*, 14(3):159–168, 1996.